A toy model of climatic variability with scaling behaviour

Demetris Koutsoyiannis

Department of Water Resources, School of Civil Engineering, National Technical University of Athens, Heroon Polytechneiou 5, GR-157 80 Zographou, Greece

(phone +30 210 772 2831, fax +30 210 772 2832, email dk@itia.ntua.gr)

Submitted to *Journal of Hydrology* for the special issue on the conference *Hydrofractals '03*; January 2004.

Revised version: August 2004.

Abstract It is demonstrated that a simple deterministic model in discrete time can reproduce the scaling behaviour of hydroclimatic processes at time scales coarser than annual, a behaviour more widely known in hydrology as the Hurst phenomenon. This toy model is based on a generalised "chaotic tent map", which may be considered as the compound result of a positive and a negative feedback mechanism, and involves two degrees of freedom. The model is not a realistic representation of a climatic system, but rather a radical simplification of real climatic dynamics. However, its simplicity helps understand the physical mechanisms that cause the scaling behaviour and simultaneously enables easy implementation and convenient experimentation. Application of the toy model gives traces that can resemble historical time series of hydroclimatic variables, such as temperature and river flow. In particular, such traces exhibit scaling behaviour with a Hurst coefficient greater than 0.5 and their statistical properties are similar to that of observed time series. Moreover, application demonstrates that large-scale synthetic "climatic" fluctuations (like upward or downward trends) can emerge without any specific reason and their evolution is unpredictable, even when they are generated by this simple fully deterministic model with only two degrees of freedom. Thus, the model emphasises the large uncertainty associated with the scaling behaviour, rather than enhances the prediction capability, despite the simple deterministic dynamics it uses, which obviously, are only a caricature of the much more complex dynamics of the real climatic system.

Keywords: climatic variability; climatic change; hydrological persistence; Hurst phenomenon; predictability; scaling; uncertainty.

1. Introduction

1.1 The notion of a toy model

According to a definition adapted from Cox and Isham (1998), a toy model is a model in which the features represented are kept to a minimum in order to show that some empirical phenomenon can or cannot be produced from primitive assumptions. The objectives of a toy model are (a) to investigate whether simple mechanisms can produce a complex phenomenon; (b) to identify essentials and discard details in the system dynamics, and (c) to identify sets of parameters for which the phenomenon occurs. Generally, in a toy model a small number of parameters are involved whose formal fitting may be irrelevant.

Several examples of toy models can be found in the literature, which cover a broad range of complex phenomena in geosciences, such as the earthquake generation (Burrige and Knopoff, 1967; Bak and Tang, 1989), the evolution of avalanches (Bak and Sneppen, 1993), the ENSO dynamics (Andrade et al., 1995), and in biosciences such as the biological evolution of species (Wandewalle & Ausloos, 1996) and the attraction of parasites and predators (Freund & Grassberger, 1992). Some of these models have become famous for their simplicity and generality.

The phenomenon studied here is the simple scaling behaviour of hydroclimatic time series in discrete time. Scaling is meant in terms of invariance properties of the time series aggregated (or averaged) on different time scales.

1.2 A simple scaling process as a stochastic process

The scaling behaviour is better expressed mathematically based on the theory of stochastic processes. Let X_i denote a hydrological or meteorological process with $i = 1, 2, \ldots$, denoting discrete time with time step or scale which for the purposes of this paper is annual or multi-annual. It is assumed that the process is stationary, a property that does not hinder to exhibit multiple scale variability. Further, let its mean be denoted as $\mu := E[X_i]$, its autocovariance

$\gamma_j := \mathrm{Cov}[X_i, X_{i+j}]$ ($j = 0, \pm1, \pm2, \ldots$), its autocorrelation $\rho_j := \mathrm{Corr}[X_i, X_{i+j}] = \gamma_j / \gamma_0$, and its standard deviation $\sigma := \sqrt{\gamma_0}$.

Let k be a positive integer that represents a timescale larger than the basic timescale of the process X_i. The aggregated stochastic process on that timescale is denoted as

$$Z_i^{(k)} := \sum_{l=(i-1)\,k+1}^{i\,k} X_l \tag{1}$$

The statistical characteristics of $Z_i^{(k)}$ for any timescale k can be derived from those of X_i. For example, the mean is

$$E[Z_i^{(k)}] = k\,\mu \tag{2}$$

whilst the variance and autocovariance (or autocorrelation) depends on the specific form of γ_j (or ρ_j). In the case examined in this paper, the process of interest exhibits simple scaling behaviour, described by the relationship,

$$(Z_i^{(k)} - k\,\mu) \overset{\mathrm{d}}{=} \left(\frac{k}{l}\right)^H (Z_j^{(l)} - l\,\mu) \tag{3}$$

where the symbol $\overset{\mathrm{d}}{=}$ stands for equality in (finite dimensional joint) distribution and H is the Hurst coefficient. This relationship holds strictly if X_i is fractional Gaussian noise (FGN; Mandelbrot, 1965), or if consecutive X_i are stationary increments of a self-similar process. Our interest here includes processes that may be not Gaussian, so we will limit the scaling property (3) to second-order properties only and we will use the term simple scaling signal (SSS) for the process. In this case, for $i = j = l = 1$ we obtain from (3) that the variance of the aggregated process is

$$\gamma_0^{(k)} := \mathrm{Var}[Z_i^{(k)}] = k^{2H}\,\gamma_0 \tag{4}$$

Thus, the standard deviation is a power law of the scale or level of aggregation k with exponent H, i.e.,

$$\sigma^{(k)} := \left(\gamma_0^{(k)}\right)^{1/2} = k^H\,\sigma \tag{5}$$

The autocorrelation function, for any aggregated timescale k, is independent of k, and given by (e.g., Koutsoyiannis, 2002)

$$\rho_j^{(k)} = \rho_j = (1/2)\,(|j+1|^{2H} + |j-1|^{2H}) - |j|^{2H} \approx H\,(2H-1)\,|j|^{2H-2} \tag{6}$$

which shows that autocorrelation is a power function of lag. Consequently, the autocovariance $\gamma_j^{(k)} = \gamma_0^{(k)}\,\rho_j^{(k)}$ is a power law of both the scale k (with exponent $2H$) and the lag j (with exponent $2H - 2$).

The power spectrum of the process

$$s_\gamma^{(k)}(\omega) = 2\sum_{j=-\infty}^{\infty} \gamma_j^{(k)} \cos(2\pi j\,\omega) \tag{7}$$

is given approximately by

$$s_\gamma^{(k)}(\omega) \approx 4\,(1-H)\,\gamma_0^{(k)}\,(2\,\omega)^{1-2H} \tag{8}$$

which is a power law of both the scale k (with exponent $2H$) and the frequency ω (with exponent $1 - 2H$).

Any of the power law equations (4), (5), (6) and (8) can be used to detect the potential simple scaling behaviour of a time series. The easiest is (5), which calls for a double logarithmic plot of standard deviation of the aggregated process $Z_i^{(k)}$ versus time scale k. In such a plot, which will be used extensively here (with the first example being illustrated in Figure 1, down) and will be called the aggregated standard deviation plot, a scaling behaviour is manifested as a straight line arrangement of points corresponding to different timescales, whose slope is the Hurst coefficient.

1.3 The hydrological importance of the scaling behaviour

It is well known that the scaling behaviour in natural processes has been discovered by Hurst (1951), while investigating the discharge time series of the Nile River. This behaviour, also termed (long-term) hydrological persistence, was essentially observed as a tendency of wet years to cluster into multi-year wet periods or of dry years to cluster into multi-year drought

periods. The terms 'Hurst phenomenon' and 'Joseph effect' (due to Mandelbrot, 1977, from the biblical story of the 'seven years of great abundance' and the 'seven years of famine') have been used as alternative names for the same behaviour. Since then, the scaling behaviour has been identified in several hydrological time series such as (to mention a few of the more recent studies) flows of several rivers such as Nile (Eltahir, 1996; Koutsoyiannis, 2002), Warta, Poland (Radziejewski & Kundzewicz, 1997), Boeoticos Kephisos, Greece (Koutsoyiannis, 2003a, b), Nemunas, Lithuania (Sakalauskienė, 2003), and Canadian streamflow series (Yue and Gan, 2004); and inflows of Lake Maggiore, Italy (Montanari et al., 1997). It was also identified in other climatological time series including wind power (Haslet & Raftery, 1989); global or point mean temperatures (Bloomfield, 1992; Koutsoyiannis, 2003a; Rust et al., 2004); indexes of North Atlantic Oscillation (Stephenson et al., 2000); and tree-ring widths, which are indicators of past climate (Koutsoyiannis, 2002).

The initial discovery of the scaling behaviour in the framework of hydrological studies is not coincidental. Rather, it manifests the strong consequences of this behaviour in water resources engineering and management. Particularly, the practical importance of the Hurst phenomenon increases in projects whose operation cycles span across long periods of time. As a typical example may serve large reservoirs with multi-year flow regulation (Klemeš et al., 1981; Koutsoyiannis 2005). However, even in hydrosystems with small reservoirs or no reservoirs at all the effect on the scaling behaviour is significant if the uncertainty (not only the expected value) of water availability is to be assessed. Since uncertainty has become a major issue in water management today (also in relation to climate changes), the Hurst phenomenon has gained new interest (e.g. Evans, 1996; Koutsoyiannis, 2003a, b; Koutsoyiannis and Efstratiadis 2004).

Specifically, if a hydrological process were random and our information on this was based on a sample of size n, then the uncertainty on the long term, which can be expressed in terms of the variance of the estimator of the mean, $\overline{X}$, would be:

$$\mathrm{var}[\overline{X}] = \frac{\sigma^2}{n} \tag{9}$$

This offers good approximation for a process with short-term persistence, as well, but it is not valid for a process with scaling behaviour. Instead, the following relation holds (Adenstedt, 1974; Beran, 1994, p. 54; Koutsoyiannis, 2003a):

$$\mathrm{var}[\bar{X}] = \frac{\sigma^2}{n^{2-2H}} \tag{10}$$

The difference between the classical statistical formula (9) and the SSS formula (10) becomes very significant for large values of H. For example, in a time series of $n = 100$ years of observations and standard deviation σ, according to the classical statistics (equation (9)), the standard estimation error, i.e. the square root of var[$\bar{X}$], is $\sigma/10$. However, for $H = 0.8$ the correct standard error, as given by equation (10), is $\sigma/2.5$, i.e. four times larger. To have an estimation error equal to $\sigma/10$, the required length of the time series would be 100 000 years! Obviously, this dramatic difference induces substantial differences in other common statistics as well (Koutsoyiannis, 2003a).

A further demonstration of the difference in uncertainty estimations between classical and SSS statistics is given in Figure 1 by means of an example taken from Koutsoyiannis and Efstratiadis (2004). The upper panel depicts a runoff time series, that of the Boeoticos Kephisos River basin, which is the longest available in Greece (96 years). The fact that the Boeoticos Kephisos River supplies water to Athens, the capital of Greece with a population approaching 5 million, makes the study of uncertainty of the runoff extremely important. The uncertainty should be assessed in several time scales, from annual to multi-year ones. Thus, apart from the annual time series plot, a plot of the 30-year moving average is also given in Figure 1 (here the averaged rather than aggregated time series, i.e. $z_i^{(30)}/30$, has been used). The 30-year time scale is typically assumed to be sufficient to smooth out the annual variations and provide values representative of the climate. The latter plot indicates a downward trend. It may be speculated that this seemingly monotonic trend may be part of a large-scale fluctuation behaviour, which in this case cannot be seen due to the limited observation time window (this will become clearer later using longer time series). Such a large scale fluctuation is none other than the scaling behaviour (Koutsoyiannis, 2002). As

mentioned above, a better means to identify the scaling behaviour is the aggregated standard deviation plot of the time series. This is plotted in Figure 1 (down), where the scaling behaviour becomes evident as a straight line arrangement of points corresponding to different timescales, whose slope is the Hurst coefficient (H = 0.79). Based on this coefficient and using the stochastic description of the scaling behaviour described above, the quantification of uncertainty can be done in terms of confidence limits that can be obtained by Monte Carlo simulation and can incorporate both the uncertainty due to unknown parameters and due to the variability of the process at each scale of interest. Such confidence limits, taken from Koutsoyiannis and Efstratiadis (2004) and referring to this example and to the 30-year (climatic) average, were plotted in Figure 1 (up), also in comparison with confidence limits estimated from classical statistics. It is observed that the confidence band has dramatically widened (almost 4 times) in the SSS case in comparison to that of the classical statistics.

In an attempt to understand what caused the scaling behaviour of this runoff time series (manifested in this case as a downward trend due to the limited observation period) one should perform a similar analysis to the rainfall time series of the same catchment. Apparently, rainfall and runoff are associated in a cause-and-effect relation. Plots of the annual rainfall time series, the 30-year moving average and its confidence bands, estimated both by classical and SSS statistics are given in the middle panel of Figure 1. Behaviour similar to that of the runoff can be observed in the rainfall time series, with a dominant downward trend. The scaling behaviour of rainfall is more evident in the lower panel of Figure 1, where the aggregated standard deviation plot of the time series shows again a straight line arrangement of points with slope H = 0.64. Thus, the scaling behaviour of rainfall may be hypothesised as a cause for the scaling behaviour of runoff. To enhance this hypothesis, a rainfall-runoff model of the catchment (Rozos et al., 2004) was fed by the rainfall series and the resulted runoff has been plotted both in annual and 30-year scale, in comparison to the measured series, in the upper panel of Figure 1. From this plot, which for the 30-year scale is practically indistinguishable from the historical one, as well as from the aggregated standard deviation plot of the modelled series, also shown in the lower panel of Figure 1, it becomes clear that the scaling behaviour of runoff is completely explained by the

similar behaviour of rainfall. The enhancement of the Hurst coefficient, from 0.64 to 0.79, is in accord to Klemeš's (1974) observation, that the output of a system grows progressively more Hurst-like with an increasing complexity of the system.

1.4 Physical explanations of the scaling behaviour

Although the scaling behaviour of hydrometeorological processes has been considered by many as mysterious, several explanations have been proposed. Most of them, however, are conceptual, rather than physical, i.e. they do not aim at explaining the physical mechanism leading to the scaling behaviour of historical records of the processes, but examine different stochastic mechanisms that might produce realizations resembling the patterns of the observed empirical time series. For example, Klemeš (1974) analyzed several variants of the 'changing mean' mechanism which assumes that the mean of the process is not a constant determined by the arithmetic mean of the record, but varies through time. Montanari et al. (1999) studied the effect of periodical patterns, as a potential cause of the Hurst phenomenon, although they note that such patterns are unusual in real data. Bhattachara et al. (1983) studied the effect of monotonic deterministic trends and showed mathematically that a trend which is a power law of time (plus a constant), results in time series exhibiting the Hurst phenomenon. We may note, however, that this kind of nonstationarity with a monotonic deterministic trend spanning the whole length of a time series can hardly represent a long time series of real data, even though in short time series may seem to be realistic. Another explanation was proposed by Koutsoyiannis (2002), who demonstrated that a Markovian underlying process at the annual scale can result in a nearly FGN process if there occur random fluctuations of the mean of the process on two different scales (e.g., tens and hundreds of years), yet the resulting composite process being stationary.

Two more physically-based model types that lead to system evolution (in time or space) with scaling properties are described by Beran (1994, pp. 16-20). The first model type applies to critical phenomena in nature such as phase transition (transition from liquid to gaseous phase, or spontaneous magnetization of ferromagnetic substances). For some critical system

temperature, the correlation of the system state at any two points decays slowly to zero, so the correlation in space can be represented by (6). The second type is related to models based on stochastic partial differential equations, which, under certain conditions, result in solutions with long-range dependence. These models provide sound links of the scaling behaviour with physics but are very complex.

In this respect, the toy model proposed in this study aims to provide a simple and easily understandable physical mechanism than can cause scaling behaviour of a hydroclimatic process. As justified above, even though the importance of the scaling behaviour rises to prominence mainly in hydrology and water resources management, its physical explanation should be sought mostly in climatic mechanisms. For this reason, the empirical basis of the study (section 2) includes climatic time series and the model formulation follows a brief description of the major climate change processes and feedbacks (section 3). The toy model is formulated by a simplification of climatic dynamics (section 4) yet being able to reproduce the scaling characteristics observed in climatic time series (section 5). Given the deterministic character of the toy model, an important potential use is to assess whether the deterministic dynamics can or cannot reduce the large uncertainty implied by the scaling behaviour, as already described in statistical terms above. This problem is explored systematically (section 6) and it is demonstrated that the model use emphasises the inherent natural uncertainty, rather than enhances the deterministic prediction capability.

2. Empirical basis of the study

The already presented time series of the Boeoticos Kephisos catchment were used here as an introductory hydrological example, mainly to demonstrate the hydrological importance of the scaling behaviour and the close relationship between scaling in rainfall and runoff. However, due to their short length (albeit much longer than typical hydrologic records used in engineering practice) they are not appropriate for further investigation. Instead, three long hydroclimatic time series are used as the main empirical basis of this study. The first series, one of the most intensively studied, is the annual minimum water level of the Nile river for the years 622 to 1284 A.D. (663 observations), measured at the Roda Nilometer near Cairo

(Toussoun, 1925, p. 366-385; Beran, 1994; available online from http://lib.stat.cmu.edu/S/beran). In Figure 2 (up) we have plotted the data values versus time, as well as the 5-year and 25-year averages versus time, which represent the aggregated processes at timescales $k = 5$ and 25, respectively. For comparison we have also plotted in Figure 2 (middle) a series of white noise with statistics same with those of the Nilometer data series. We can observe that the fluctuations of the aggregated processes, especially for $k = 25$, are much greater in the real world time series than in the white noise series. These fluctuations could be taken as nonstationarities, that is, deterministic rising or falling trends that last 100-200 or more years. For example, if one had available only the data of the 100-year period 700-800 one would detect a 'deterministic' falling trend of the Nile level (as happened in the 96-year Boeoticos Kephisos data series); similarly, one would detect a regular rising trend of the Nile level between the years 1000-1100. However, the complete picture of the series suggests that these trends are parts of large-scale random fluctuations rather than monotonic trends, thus pointing out to the scaling behaviour of the series. The scaling behaviour is more evident in the aggregated standard deviation plot of Figure 2 (down), where we have also plotted for comparison theoretical curves for the white noise (in which the standard deviation is proportional to the square root of scale) and the FGN model (for which equation (5) holds) for $H = 0.85$. Clearly, the empirical plot is virtually identical to the theoretical FGN plot and departs significantly from the plot corresponding to the white noise, whose slope equals 0.5.

The second series, the Jones data series (available from ftp.ngdc.noaa.gov/paleo/contributions_by_author/jones1998/), represents the Northern Hemisphere temperature anomalies for 992 years (in °C) with reference to 1961–1990 mean. This series was constructed by Jones et al., (1998) using temperature sensitive paleoclimatic multi-proxy data from 10 sites worldwide that include tree rings, ice cores, corals, and historical documents. Only four of the proxy data series go back before 1400 AD and, therefore, data prior to about 600 years ago are more uncertain. This series has been plotted in Figure 3 (up) and its scaling properties (which have been also studied earlier; Koutsoyiannis, 2003a), are evident from the aggregated standard deviation plot of Figure 3 (down). The Hurst coefficient is 0.88 for the

total series and, notably, it does not change if the data values of the 20th century, which may incorporate anthropogenic influence, are excluded.

The third example, the Vostok data series (available from http://www1.ncdc.noaa.gov /pub/data/paleo/icecore/antarctica/vostok/deutnat.txt), is the temperature difference with reference to the mean recent time value as estimated from the Vostok ice core deuterium data set that goes back to 422 766 years before present (Petit et al., 1999). This temperature difference is calculated based on the deuterium content of the ice using a deuterium/temperature gradient of 9‰/°C, after accounting for the isotopic change of sea-water. The temporal resolution ranges from 17 years (present time) to 631 years. Here the series was re-interpolated using a constant 400 year temporal resolution. The time series is shown in Figure 4 (up) and its aggregated standard deviation plot is shown in Figure 4 (down), where a scaling behaviour with a scaling coefficient 0.94 is observed.

A more careful analysis of the Vostok time series reveals inherent periodicities. Indeed the periodogram $s(\omega)$ (the estimate of the power spectrum defined in (7)), which is depicted in Figure 5, has peaks at frequencies 9.5×10^{-6}, 2.6×10^{-5} and 3.5×10^{-5} years^{-1} or periods of about 105 000, 38 500 and 28 500 years, respectively. These periods approximately correspond to the well-known Milankovitch cycles of Earth's orbital stretch, axial tilt and axial path wobble, respectively. The magnitudes of the peaks, which indicate the percentage of variance explained by the corresponding cycles, are $s(\omega)/(n\,\sigma^2)$ = 37%, 8.4% and 4.4%, respectively, where n is the record length (= 1061) and σ^2 is the variance (= 7.81 $^{o}C^2$).

In an attempt to describe the periodic behaviour of the series, for the first cycle we fitted by least squares the equation

$$\tilde{x}_t = 3.917 \cos(2\pi\, t/\tau + 0.2146) - 4.856 \qquad (11)$$

where τ = 103 598 years. This principal harmonic is depicted in Figure 6 (up) in comparison with the original series. This harmonic is then subtracted from the original series and the resulting series is plotted in Figure 6 (middle). In this, the variance σ^2 is reduced by 25% (it becomes 5.88 $^{o}C^2$) and still the frequency 9.5×10^{-6} explains a great percentage (20%) of the reduced variance (15% of the initial variance). The other two peak frequencies (2.6×10^{-5} and

3.5×10^{-5} years^{-1}) explain smaller percentages of the reduced variance (11% and 5.6%) so their subtraction is aimless. The aggregated standard deviation plot of the adapted series is shown in Figure 6 (down), where no significant change, in comparison with Figure 4 (down), is observed, so the scaling coefficient continues to be 0.94. The scaling behaviour is also observed in Figure 5 (right), where the periodogram appears to be a power law of frequency (note that the subtraction of the harmonic does not create significant changes in double logarithmic plot of the periodogram).

3. Major climate change processes and feedbacks

The Milankovitch cycles are known periodical effects on the climate, which can be considered as external forcings. Other external forcings, such as changes in solar irradiance and the volcanic activity have significant effect on climate. In addition, there exist internal climatic mechanisms related to the composition of the atmosphere and the ocean-atmosphere-land interactions, which act as feedback controls either amplifying change (positive feedbacks) or producing stability (negative feedbacks). Some well known examples easy to understand (e.g. Moran and Morgan, 1997, pp. 484-485) are the ice-albedo feedback (temperature increase → ice melt → decrease of albedo → temperature increase; i.e., positive feedback), the water vapour feedback (temperature increase → greater evaporation → more vapour in the atmosphere, which is a greenhouse gas → decrease of infrared radiation leaving Earth → temperature increase; i.e., positive feedback), and the low cloud feedback (temperature increase → greater evaporation → more low clouds in the atmosphere, which are highly reflective → increase of albedo → temperature decrease; i.e., negative feedback).

Biosphere plays also an important role in climate as it creates its own feedbacks. Even the effect of biosphere to the albedo of land surface may be very significant as demonstrated by Watson and Lovelock (1983) in their well-known ‘Daisyworld’ parable. However, the effect of biosphere may be much more complex as articulated by Lovelock (1982) in his Gaia hypothesis, which claims that the Earth is a self organising Cybernetic system, in which the living matter, atmosphere, ocean, and land surfaces interact to keep the Earth a fit place for life.

Obviously, the interaction of all climatic mechanisms is extremely complex and its detailed mathematical representation is difficult task. To construct a toy model, however, the accurate description of mechanisms is not necessary but rather, according to the definition given in the Introduction, a minimum of key mechanisms should be taken into account in order to show that the phenomenon studied, the climatic scaling behaviour, can or cannot be produced from these key mechanisms. In this respect, it suffices to explore the general behaviour that a synthesis of positive and negative reactions in a feedback loop may produce. In this attempt we will ignore the external forcings and we will use a simple systems approach in discrete time.

The dynamics of a system, expressed in discrete time, is a transformation $x_t = F(x_{t-1})$ of the previous system state x_{t-1} to the current state x_t. Generally the system state is represented by a vector but in our examples it suffices to consider the system state as a scalar (e.g. the temperature anomaly in the Jones and Vostok cases or the minimum river level in the Nile case). A system state x^* satisfying $x^* = F(x^*)$ is a fixed (or stationary) point of the transformation. The transformation F is usually the compound effect of several system components performing their separate transformations. These are linked together in a loop or network, whose branches and connections represent the interaction of components. A comprehensive presentation of systems with feedback components and their mathematical analysis is contained, among others, in Oppenheim et al. (1983).

A simple system that will be used as an extremely simplified representation of the climatic system is depicted in Figure 7. The boxes in this figure can be thought of as components (reactions) of the system that transform their inputs to obtain their outputs. The component transformation is determined by multiplying the input by the so called gain value, which is depicted over each component in Figure 7. The entire system is a loop containing a forward component with gain 1 and two reaction components connected in series in a feedback path, one positive with gain f_1 and one negative with gain f_2. The positive feedback is characterised by a gain for which $|1 - f_1| \leq 1$, whereas the negative feedback is characterised by $|1 - f_2| \geq 1$ (Mitchel, 2003). Further, we will assume that the feedback components of the system are

nonlinear, so that the gains are functions of the previous system state x_{t-1} (i.e., $f_1(x_{t-1})$ and $f_2(x_{t-1})$, respectively).

In the absence of the feedback path of the system, its operation is the simplest possible: the output $O = x_t - x^*$ equals the input $I = x_{t-1} - x^*$, i.e. no change occurs since the forward gain is 1 (immobility). Under the action of one of the two components with gain $f_i(x_{t-1})$ (i = 1 or 2), it is easy to see that the input of the forward component is the sum of the system input $x_{t-1} - x^*$ and the feedback, which is the product of the output $O = x_t - x^*$ and the gain $f_i(x_{t-1})$. Equating the input and output of the forward component, we easily obtain that the system dynamics is

$$x_t = x^* + (x_{t-1} - x^*) / [1 - f_i(x_{t-1})] \tag{12}$$

For example, if $f_i(x_t - 1) = 0.5$, which represents a positive feedback since $|1 - f_i(x_{t-1})| \leq 1$, then (12) yields $x_t - x^* = 2\,(x_{t-1} - x^*)$, so the deviation from the fixed point is doubled at each time step. This soon will lead the system to the so called runaway situation. If $f_i(x_{t-1}) = \infty$, which is a negative feedback since $|1 - f_i(x_{t-1})| \geq 1$, then (12) yields $x_t = x^*$, so the system is brought to its fixed point regardless of the previous state x_{t-1} (complete stability). If $f_i(x_{t-1}) = 0$, which in fact is absence of feedback, the example system is characterised by immobility.

The system behaviour becomes more interesting if both reactions operate simultaneously. It is easily obtained that the compound effect of the two components results in the system dynamics:

$$x_t = x^* + (x_{t-1} - x^*) / [1 - f_1(x_{t-1})\, f_2(x_{t-1})] \tag{13}$$

Figure 8 depicts a numerical example of (13), for a system whose state ranges between 0 and 1. The first reaction is assumed to follow the simple symmetrical form

$$f_1(x) = \min(x, 1 - x) \tag{14}$$

with a maximum value $f_1(0.5) = 0.5$ so that $|1 - f_1(x)| \leq 0.5$ which secures that the feedback is positive. The second one is chosen in a manner that the compound effect of both is symmetric and covers the whole range [0, 1]:

$$f_2(x) = \frac{3}{\min(6x - 2, 2 - 2x)} \tag{15}$$

The minimum value of $|1 - f_2(x)| = 2$ (for $x = 0.5$) which secures that the feedback is negative. The fixed point is assumed to be $x^* = 2/3$. The resulting, according to transformation (12), system dynamics for each of the reactions are depicted in Figure 8 (up). It can be easily shown that the synthesis of the two feedback components given by (13) yields to the so called tent transformation

$$x_t = 2 \min(x_{t-1}, 1 - x_{t-1}) \tag{16}$$

which, as also depicted in Figure 8 (up), has an upward and a downward segment. It can be easily shown that the compound feedback is negative for $x \leq x^{*2} = 4/9$ and positive for $x \geq 4/9$. Apparently, such a form with an upward and a downward segment may appear for other combinations of $f_1(x_{t-1})$ and $f_2(x_{t-1})$ or for other topologies of the control loop. For example, it could be obtained from a control loop with a forward component with gain greater than 1 (so that any deviation from the fixed point is amplified) and a single negative feedback component. However, it was preferred to derive it as the compound effect of two reaction components, acting in series (and thus in a multiplicative manner) as shown in Figure 7, because the derived system is simpler (e.g. mathematically equivalent and interchangeable f_1 and f_2).

On the other hand, a form with an upward and a downward segment does not appear for any functions $f_1(x_{t-1})$ and $f_2(x_{t-1})$; it could be a constantly increasing or decreasing curve, but the existence of both increasing and decreasing segments is a better choice for a toy model as it makes the completely stable or the runaway behaviour of the system less likely. Figure 8 (down) depicts such an evolution for an initial state $x_0 = 0.67$ very close to the fixed point, $x^* = 2/3$. The negative reaction acting alone brings the system immediately to its fixed point exactly and keeps it steadily to this state. The positive reaction acting alone leads the system to a runaway behaviour, which in this case is represented by $x = 1$ (had the initial state be lower than 2/3, the runaway behaviour would be represented by $x = 0$). The synthesis of both

reactions leads the system to oscillate in an erratic rhythm, so it creates a more "realistic" trajectory of the system.

4. The toy model

The above example provides some insight on the causes of erratic behaviour but it is too simple to capture the scaling behaviour. Therefore, some steps of generalisation are needed to construct a more realistic toy model. In the first step we add one parameter (α) to the transformation (16) to get the generalised tent map:

$$x_t = g(x_{t-1};\, \alpha) := \frac{(2-\alpha)\,\min\,(x_{t-1},\, 1-x_{t-1})}{1-\alpha\;\;\min\,(x_{t-1},\, 1-x_{t-1})} \tag{17}$$

with $0 \le x_t \le 1$ and $\alpha < 2$. For $\alpha = 0$, (17) is reduced to (16) but still for $\alpha \neq 0$ it keeps the symmetry of (16) and the upward-downward segments. Figure 9 depicts (17) for different values of its parameter α. The generalised tent map has been used in the study of dynamical systems. For example, the map approximates the relation between successive maxima in the variable $x(t)$ from the Lorenz equations that describe climatic dynamics (Lasota and Mackey, 1994, p. 150).

More complex maps result from successive applications of generalised tent map, i.e.,

$$x_t = g_n(x_{t-1};\, \alpha) := \underbrace{g(g(\ldots(g(x_{t-1};\, \alpha)\ldots);\, \alpha);\, \alpha)}_{n} \tag{18}$$

Equivalently, the transformation $g_n(\,)$ can be defined from

$$x_t = y_{n\,t}, \quad y_{n\,t} = g(y_{n\,t-1};\, \alpha),\;\; y_0 = x_0,\; t = 0,\, 1,\, 2,\, \ldots \tag{19}$$

where the intermediate terms $y_{(n-1)t+1},\ \ldots\ \ y_{n\,t-1}$ are regarded as hidden terms. Figure 10 demonstrates the transformation $g_n(x;\, \alpha)$ for $n = 4$ and $\alpha = 1$, which has eight upward and eight downward segments.

A time series generated by the transformation $g_n(x;\, \alpha)$ displays random appearance of the series at the basic scale and stabilising behaviour at larger scales, which is manifested by a Hurst coefficient equal to 0.5. This behaviour is observed for any $\alpha < 1$ (a dwarf scaling

behaviour but with unrealistic shape appears for α between 0.99 and 1), whereas for $\alpha > 1$ a runaway behaviour is observed. Thus, the generalised tent map is not an appropriate toy model for our purpose, as it does not exhibit the scaling property sought with Hurst exponent greater than 0.5. However, it becomes appropriate if we make its parameter α time dependent, assuming that its temporal evolution is described again by the same tent transformation. The resulting compound transformation, which we will call the double tent transformation, is given by

$$u_t = G(u_{t-1}, \alpha_{t-1}; \kappa, \lambda) := g(u_{t-1}; \kappa\, \alpha_{t-1}), \quad \alpha_t = g(\alpha_{t-1}; \lambda) \tag{20}$$

We also extend this transformation by adding hidden terms thus getting

$$u_t = y_{n\,t}, \quad y_{n\,t} = G(y_{n\,t-1}, \alpha_{n\,t-1}; \kappa, \lambda), y_0 = u_0, t = 0, 1, 2, \ldots \tag{21}$$

Both parameters κ, λ should be smaller than 2 whereas the domain of u_t is the interval [0, 1]. This domain is not appropriate for climatic variables. Thus we apply an additional rescaling transformation to shift from [0, 1] to $[b, \infty)$ (for some b positive, negative or zero):

$$x_t = b + c\, [\tan(\pi\, u_t / 2)]^d \tag{22}$$

The final model for x_t, which will be our toy model sought, is two dimensional, as it involves two degrees of freedom corresponding to the initial conditions (α_0, u_0), and contains five real valued parameters (κ, λ, b, c, d) and one integral parameter (n). Among these, the most important, which determine the scaling behaviour of the model, are the parameters of the double tent transformation κ and λ. The model behaviour with respect to these parameters has been investigated numerically and the results are depicted in Figure 11. We observe that for small values of the parameter κ, the time series synthesised by the model do not exhibit scaling behaviour but, rather, they have Hurst coefficient 0.5. For large values of κ, the model yields a runaway behaviour. In between the two non-interesting areas, the non-scaling and the runaway, there is an area of parameter values, shaded in Figure 11, in which the resulting time series exhibit the scaling behaviour sought; this area shrinks for increasing n, but still does not disappear as shown in Figure 11. This will be used further in the application of the toy model

with the example time series. All three types of behaviour are observed for negative values of λ (not shown in Figure 11) whereas for $\lambda > 1$ only the runaway behaviour is observed regardless of the value of κ.

5. Model application

The model application with the example data sets contains two steps: the estimation of parameters (fitting of the toy model) and the comparison of statistical properties (with emphasis on the scaling behaviour) of the original and the synthesised by the toy model series.

Due to the deterministic character of the model, the estimation of parameters is done in a manner similar to that usually used in fitting deterministic models rather than in stochastic models. It is reminded that in stochastic modelling the preservation of the particular data values forming the time series is irrelevant, so certain summary statistics are derived and subsequently used in the model fitting. In contrast, in deterministic modelling the aim is to reproduce the particular data values of the time series as faithfully as possible. What differs here from typical deterministic models (e.g. rainfall-runoff models) is the absence of an input time series. As usual, parameter estimation can be regarded as a typical optimisation problem, in which the objective is to obtain the optimal fitting by appropriate choice of the values of the unknown parameters and the unknown initial conditions. Due to the sensitive dependence of the toy model on its parameters and initial conditions, a random search technique is the most appropriate to determine the values of unknowns. The criterion set for the model fitting is to obtain large correlation of a series generated by the model for the specified parameter set with the historical series both for the basic time scale (1 time step) and an aggregated time scale (chosen to be 50 time steps). Equal weights were assumed for the correlations of both time scales. The random search procedure requires a large number of repetitions. In each repetition, the parameters, κ, λ, d and the initial conditions α_0, u_0 are generated at random from their appropriate domains. A time series is then generated assuming that the additional parameters b and c are respectively 0 and 1 and then the values of these parameters are

estimated by linear regression between historical and generated series. After a large number of repetitions, the parameter set with the greatest value of the fitting criterion set is chosen.

The second step (comparison) includes statistical comparisons of the generated and historical series, in terms of the marginal distribution, the temporal structure expressed by the autocorrelation function, and finally the scaling behaviour, which is the focus of the study, expressed by the aggregated standard deviation plot.

Table 1 lists the parameter values and initial values of the toy model fitted to the three example time series. In all cases the integral parameter was assumed to be $n = 4$. Figure 12 shows the synthetic time series generated by the toy model fitted to the Nilometer series (upper panel) and a comparison of this series with the historical one in terms of their 50-year moving averages. Figure 13 shows graphical comparisons of the statistical properties of the original Nilometer time series and the synthetic one in terms of distribution function (upper panel), autocorrelogram (middle panel) and aggregated standard deviation plot (lower panel). It is generally observed that the resemblance of the statistical characteristics including the scaling behaviour is impressively good, despite the simplicity and the deterministic character of the toy model.

Similarly, good performance can be observed for the other two cases. The results for the Jones data set are shown in Figure 14 (time series) and Figure 15 (comparisons). The application to the Vostok data set was based initially on the adapted time series (with the principal harmonic subtracted) and the results are shown in Figure 16 (time series) and Figure 17 (comparison). Then the harmonic of equation (11), which should be regarded as an external effect not related to the internal feedback mechanisms, was added to the time series of Figure 16. The resulting time series is shown in Figure 18 whereas the comparisons of its characteristics with those of the original Vostok time series are shown in Figure 19.

6. The emergence of uncertainty in a deterministic context

The above examples show that the toy model is good enough to generate climatic sequences that resemble the actual ones, despite its simplicity and low dimensionality. The entire model involves no randomness at all and given the values of parameters and initial conditions it

gives a unique evolution. Given the deterministic character of the model, one may think of utilising it to forecast future climate. We will demonstrate here that this is structurally impossible.

In the preceding examples of synthetic time series the initial conditions were generated at random. In a forecast framework, however, the initial values u_0 and α_0 should be estimated so that the synthetic series match the historical ones at the most recent two values. Having this in mind and referring to the Jones data set we have generated, in addition to the already discussed series which is referred to as synthetic series 1, two additional series referred to as synthetic series 2 and 3, which both match the historical values at the first two years (1000 and 1001). The initial values for synthetic series 2 are $u_0 = 0.70375$ and $\alpha_0 = 0.3164$ while for synthetic series 3 the same u_0 was used but the value of α_0 was assumed very faintly different, i.e. greater by only 0.00001% than that of the synthetic series 2. This difference of course is not visible in terms of matching the two initial historical values, but yields visible effects with the grow of time, as shown in Figure 20 (up), where the first 50 years of evolution of the two synthetic time series and the historical Jones series have been plotted. The difference of both synthetic series from the historical one is visible from even the first "forecast" time step (year 1002) and the two synthetic series deviate from each other three time steps later (year 1005).

Now, we will assume that the synthetic series 2 is a forecast of the actual evolution, represented by the historical series, and will assess the forecast capability by comparing it to the simplest pure statistical forecast method, according to which the forecast for any time step is given as a constant value which is the time average of the historical or simulated series. Here the average of the first 50 terms of synthetic series 2 was used as the statistical forecast. The comparison of the two methods is given graphically in Figure 20 (middle), where it becomes clear that the statistical method outperforms the deterministic one. The standard forecast error of the statistical method (0.25^{o}C) is smaller than that of the deterministic one (0.31^{o}C).

One may attribute the poor forecast capability of the deterministic model to the fact that the deterministic toy model is a poor model of reality. So, let us pretend that the actual evolution of the time series of interest is not given by the historical series but by synthetic

series 3, for which the toy model is perfect, since it was used to generate it. Based on this, we repeated the experiment shown in Figure 20 (middle) and the new experiment is depicted in Figure 20 (down). The deterministic forecast capability is not improved (in fact it gets worse as the standard forecast error becomes 0.39), and the statistical forecast still is better (standard forecast error 0.26) except for the first three to four terms. It should be noted that the statistical forecast capability can be improved at small lead times by utilising the high autocorrelation (0.67 for lag one), which was not taken into account here.

If forecast is so difficult for annual values, even though they are generated by the extremely simplified toy model, the situation becomes even more discouraging if "climate" values are to be predicted. Assuming as usual that a climatic value is the average of the past 30 annual values, we have plotted in Figure 21 (up) the climatic values of the Jones series and those of synthetic series 2 and 3. Series 2 and 3 are not closer to each other than they are to the historical series, despite the fact that they were generated by the same model with the same parameters and virtually the same initial values. Interestingly, in their origins, the historical climate and the synthetic climate 2 coincide and both have upward trends. At the same time the synthetic climate 3 starts 0.2^{o}C higher than synthetic climate 2 and follows a downward trend thereafter. None of the two synthetic climates captures the upward trend in the recent years, whereas, as shown in Figure 14 (up) this behaviour was well described by synthetic series 1. It should be emphasised, however, that both synthetic series 2 and 3, despite the different climate evolution they imply, still resemble the statistical behaviour of the historical series, as happened with synthetic series 1, and especially resemble the scaling behaviour characterised by a Hurst coefficient 0.88. The latter is depicted in Figure 21 (down).

The preservation of the scaling behaviour was further explored by extending the length of synthetic series 1 from 1000 to 12 000 "years" (Figure 22, up). Several segments of the extended series with various lengths were used to explore this behaviour and it was found that the statistical characteristics and especially the Hurst exponent do not depend seriously on length or location within time series (Figure 22, down).

In conclusion, the toy model although structurally deterministic behaves like a stochastic model as it resembles statistical characteristics without enhancing the forecast capability. This indicates that the great uncertainty associated with scaling behaviour, which was described in stochastic terms in the Introduction, may not at all decrease even if we construct a deterministic model capable of reproducing historical hydroclimatic series and the scaling behaviour thereof. This may not be a peculiarity or weakness of this particular toy model since, as von Storch et al. (2001) put it, "climate must be considered as a stochastic system, and our climate simulation models as random number generators". Indeed, determinism is very hard to trace in series generated by the toy model. To demonstrate this, we used the standard method of detecting determinism in a time series (Grassberger and Procaccia, 1983; Kantz and Schreiber, 1997; Koutsoyiannis and Pachakis, 1996). This is based on the correlation sum $C_2(\varepsilon, m)$ and its local slope $d_2(\varepsilon, m)$, where ε is the scale length and m the embedding dimension. The technical details of the algorithm can be found in the references listed above. In our case, since the toy model has dimension $D = 2$, we would expect that an embedding dimension $m = 2D + 1 = 5$ at most would suffice to reconstruct the dynamics from a time series and that the local slope $d_2(\varepsilon, m)$ would saturate at the value $D = 2$ for $m \geq 5$ and it would have values ≤ 2 for $m < 5$. The correlation sums $C_2(\varepsilon, m)$ and their local slopes $d_2(\varepsilon, m)$ estimated from the extended 12 000-year synthetic time series 1 of Figure 22 (corresponding to the Jones data set) have been plotted in Figure 23 vs. the scale length ε for embedding dimension m = 1 to 8. Clearly, no saturation of slope appears and local slopes greater than 2 emerge. That is, the standard algorithm fails to capture the low dimensional determinism in the produced series and deems it as a random series. The reason for this is the fact that the method requires tremendously high lengths of time series to work and the length of 12 000 of our case is too short for the algorithm, simultaneously being extremely and unrealistically high if compared to typical sizes of climate records.

7. Synopsis and conclusions

The Hurst phenomenon, which has been identified to be omnipresent in long hydrological time series, should be attributed to the scaling behaviour of climatic processes that stimulate

the hydrological cycle. This scaling behaviour is associated to the irregular changes (upward and downward fluctuations) on all time scales, given that "Climate changes irregularly, for unknown reasons, on all timescales" (National Research Council, 1991, p. 21).

Synthetic time series with scaling behaviour are typically generated by appropriate stochastic models. However, the idea of using a simple deterministic toy model to generate time series with scaling behaviour may be attractive as it can serve as a physical explanation of the causes of the scaling behaviour and provide some insights for the system examined. Based on this and assuming that the climatic system, which in fact incorporates atmospheric and hydrological processes, is characterised by the action of several feedback mechanisms, a simple climatic toy model was constructed. This toy model is based on the chaotic tent map, which may represent the compound result of a positive and a negative feedback mechanism. The simplicity of the deterministic toy model enables easy implementation, even on a spreadsheet environment, and convenient experimentation. Obviously, however, the toy model should not be thought of as an operational tool for climate modelling and predictions.

Application of the toy model gives traces that can resemble historical climatic time series. In particular, they exhibit scaling behaviour with a Hurst exponent greater than 0.5, thus suggesting that even simple mechanisms based on few internal components of the climate system are enough to result in a perpetually changing climate. Moreover, application demonstrates that large-scale synthetic "climatic" fluctuations can emerge without any specific reason and their evolution is uncertain and unpredictable, even when they are generated by this simple model with the caricature, purely deterministic, dynamics with only two degrees of freedom. Obviously, the fact that such a simple model can generate time series that are realistic surrogates of real climatic series does not mean that the real climatic system involves that simple dynamics. In contrast, the dynamics of the real climate system is greatly more complex than in this simple toy model.

Acknowledgements: The author is grateful to two anonymous reviewers for their comments, which helped to significantly improve presentation,

References

Adenstedt, R. K., 1974, On large sample estimation for the mean of a stationary random sequence, *Ann. Statist.*, 2, 1095–1107.

Andrade, J.S. Jr., I. Wainer, J. Mendes Filho and J.E. Moreira, 1995, Self-organized criticality in the El Niño Southern Oscillation, *Physica A*, 215, 331-338.

Bak P. and Sneppen K., 1993, Punctuated equilibrium and criticality in a simple model of evolution, Phys. Rev. Let. 74, 4083-4086

Bak, P. and C. Tang, 1989, Earthquakes as self-organized critical phenomena, *J. Geophys. Res., 94*, 15635-15637.

Beran, J., 1994, *Statistics for Long-Memory Processes*, vol. 61 of Monographs on Statistics and Applied Probability. Chapman & Hall, New York, USA.

Bhattacharya, R, N., Gupta, V. K. and Waymire, E., 1983, The Hurst effect under trends, *J. Appl. Prob.*, 20, 649–662.

Bloomfield, P., 1992, Trends in global temperature, *Climate Change*, 21, 1-16.

Burridge, R. and L. Knopoff, 1967, Model and theoretical seismicity, *Bull. Seis. Soc. Am., 57*, 341-371.

Cox, D. R., and V. Isham, 1998, Stochastic spatial-temporal models for rain, in *Stochastic Methods in Hydrology: Rain, Landforms and Floods*, edited by O.E. Barndorff-Nielsen, V.K. Gupta, V. Pérez-Abreu and E. Waymire, pp. 1-24, World Scientific, Singapore.

Eltahir, E. A. B., 1996, El Niño and the natural variability in the flow of the Nile River, *Water Resources Research*, 32(1) 131-137.

Evans, T. E. (1996), The effects of changes in the world hydrological cycle on availability of water resources. In: *Global Climate Change and Agricultural Production: Direct and Indirect Effects of Changing Hydrological, Pedological and Plant Physiological Processes* (ed. by F. Bazzaz and W. Sombroek), Chapter 2, FAO and John Wiley, Chichester, West Sussex, UK.

Freund, H., and P. Grassberger, 1992, The Red Queen's walk, *Physica A*, 190, 218-237.

Grassberger, P., and I. Procaccia, 1983, Characterization of strange attractors, *Phys. Rev. Lett.*, *50*(5), 346-349.

Haslett, J., & A. E. Raftery, 1989, Space-time modelling with long-memory dependence: Assessing Ireland's wind power resource, *Appl. Statist.*, 38(1), 1-50.

Hurst, H. E., 1951, Long term storage capacities of reservoirs, *Trans. ASCE*, 116, 776-808.

Jones, P. D., Briffa, K. R., Barnett, T. P. & Tett, S. F. B., 1998, High-resolution paleoclimatic records for the last millennium: interpretation, integration and comparison with General Circulation Model control-run temperatures. *Holocene* **8**(4), 455–471.

Kantz, H., and T. Schreiber, 1997, *Nonlinear Time Series Analysis*, Cambridge University Press, Cambridge.

Klemeš, V., 1974, The Hurst phenomenon: a puzzle? *Wat. Resour. Res.*, 10(4), 675–688.

Klemeš, V., Sricanthan, R. and McMahon T.A., 1981, Long-memory flow models in reservoir analysis: What is their practical value? *Water Resources Research*, l7(3), 737-75l.

Koutsoyiannis, D., 2002, The Hurst phenomenon and fractional Gaussian noise made easy, *Hydrol. Sci. J.*, 47(4), 573-596.

Koutsoyiannis, D., 2003a, Climate change, the Hurst phenomenon, and hydrological statistics, *Hydrological Sciences Journal*, 48(1), 3-24.

Koutsoyiannis, D., 2003b, Hydrological statistics for engineering design in a varying climate, *EGS-AGU-EUG Joint Assembly, Geophysical Research Abstracts, Vol. 5, Nice, April 2003*, European Geophysical Society, American Geophysical Union (http://www.itia.ntua.gr/g/docinfo/565/).

Koutsoyiannis, D., 2005, Reliability concepts in reservoir design, *The Encyclopedia of Water*, edited by J. H. Lehr, Wiley, New York (in press).

Koutsoyiannis, D., and Efstratiadis, A., 2004, Climate change certainty versus climate uncertainty and inferences in hydrological studies and water resources management, *1st General Assembly of the European Geosciences Union, Geophysical Research Abstracts*, Vol. 6, Nice (http://www.itia.ntua.gr/g/docinfo/606/).

Koutsoyiannis, D., and D. Pachakis, 1996, Deterministic chaos versus stochasticity in analysis and modeling of point rainfall series, *Journal of Geophysical Research-Atmospheres,* 101(D21), 26444-26451.

Lasota, A., and M.C. Mackey, 1994, *Chaos, Fractals and Noise, Stochastic Aspects of Dynamics*, Springer-Verlag.

Lovelock, J., 1982, Gaia: A New Look at Life on Earth, Oxford University Press.

Mandelbrot, B. B., 1965, Une class de processus stochastiques homothétiques a soi: Application a la loi climatologique de H. E. Hurst, *Compte Rendus Académie Science*, 260, 3274-3277.

Mandelbrot, B. B., 1977, *The Fractal Geometry of Nature*, Freeman, New York, USA.

Mitchell, R., 2003, Introduction to feedback systems, Lecture notes, Department of Cybernetics, University of Reading, (http://www.cyber.rdg.ac.uk/people/R.Mitchell /feedback/index.htm).

Montanari, A., R. Rosso & M. S. Taqqu, 1997, Fractionally differenced ARIMA models applied to hydrologic time series, *Water Resour. Res.*, 33(5), 1035-1044.

Montanari, A., Taqqu, M.S. and Teverovsky, V., 1999, Estimating long-range dependence in the presence of periodicity: an empirical study. *Mathematical and Computer Modeling*, 29, 217-228.

Moran, J. M. and M. D. Morgan, 1997, *Meteorology: the Atmosphere and the Science of Weather*, Prentice-Hall, London.

National Research Council, 1991, *Opportunities in the Hydrologic Sciences*, National Academy Press, Washington DC, USA.

Oppenheim, A. V., A. S. Willsky and I. T. Young, 1983, *Signals and Systems*, Prentice-Hall, London.

Petit J.R., Jouzel J., Raynaud D., Barkov N.I., Barnola J.M., Basile I., Bender M., Chappellaz J., Davis J., Delaygue G., Delmotte M., Kotlyakov V.M., Legrand M., Lipenkov V., Lorius C., Pépin L., Ritz C., Saltzman E., Stievenard M., 1999, Climate and atmospheric history of the past 420,000 years from the Vostok ice core, Antarctica, *Nature*, 399, 429-436.

Radziejewski, M., & Z. W. Kundzewicz, 1997, Fractal analysis of flow of the river Warta, *J. of Hydrol.*, 200, 280-294.

Rozos, E., A. Efstratiadis, I. Nalbantis and D. Koutsoyiannis, 2004, Calibration of a semi-distributed model for conjunctive simulation of surface and groundwater flows, *Hydrological Sciences Journal* (in press).

Rust, H., D. Maraun, J. Kropp and J. Timmer, 2004, Power-law scaling and long-range correlations in temperature records. *Geophysical Research Abstracts*, Vol. 6, 00298.

Sakalauskienė, G., 2003, The Hurst Phenomenon in Hydrology, *Environmental Research, Engineering and Management*, 3(25), 16-20.

Stephenson, D. B., V. Pavan & R. Bojariu, 2000, Is the North Atlantic Oscillation a random walk?, *Int. J. Climatol.*, 20, 1-18.

Toussoun, O.,1925, Mémoire sur l'histoire du Nil, in *Mémoires a l'Institut d'Egypte*, vol. 18, pp. 366-404.

von Storch, H., J-S. von Storch and P. Müller, 2001, Noise in the climate system – ubiquitous, constitutive and concealing, in *Mathematics Unlimited – 2001 and Beyond*, edited by B. Engquist and W. Schmid, Springer, Berlin.

Wandewalle, N., and M. Ausloos, 1996, A toy model for life at the "edge of chaos", *Comput. & Graphics*, 20(6), 921-923.

Watson, A. J., and J. E. Lovelock, 1983, Biological homeostasis of the global environment: the parable of Daisyworld, *Tellus*, 35B, 284-289.

Yue, S. and T. Y. Gan, 2004, Simple scaling properties of Canadian annual average streamflow, *Advances in Water Resources*, 27, 481-495.

Tables

Table 1 Parameters and initial values of the toy model fitted to the three example time series.

	Fitted parameters					Initial values	
Data set	κ	λ	b	c	d	u_0	α_0
Nilometer	1.871	0.477	-26871.1	28130.5	0.0013	0.030	0.335
Jones	1.765	0.317	73.3	-73.8	0.0013	0.797	0.325
Vostok	1.810	0.332	624.8	-628.6	0.0011	0.988	0.327

Figures

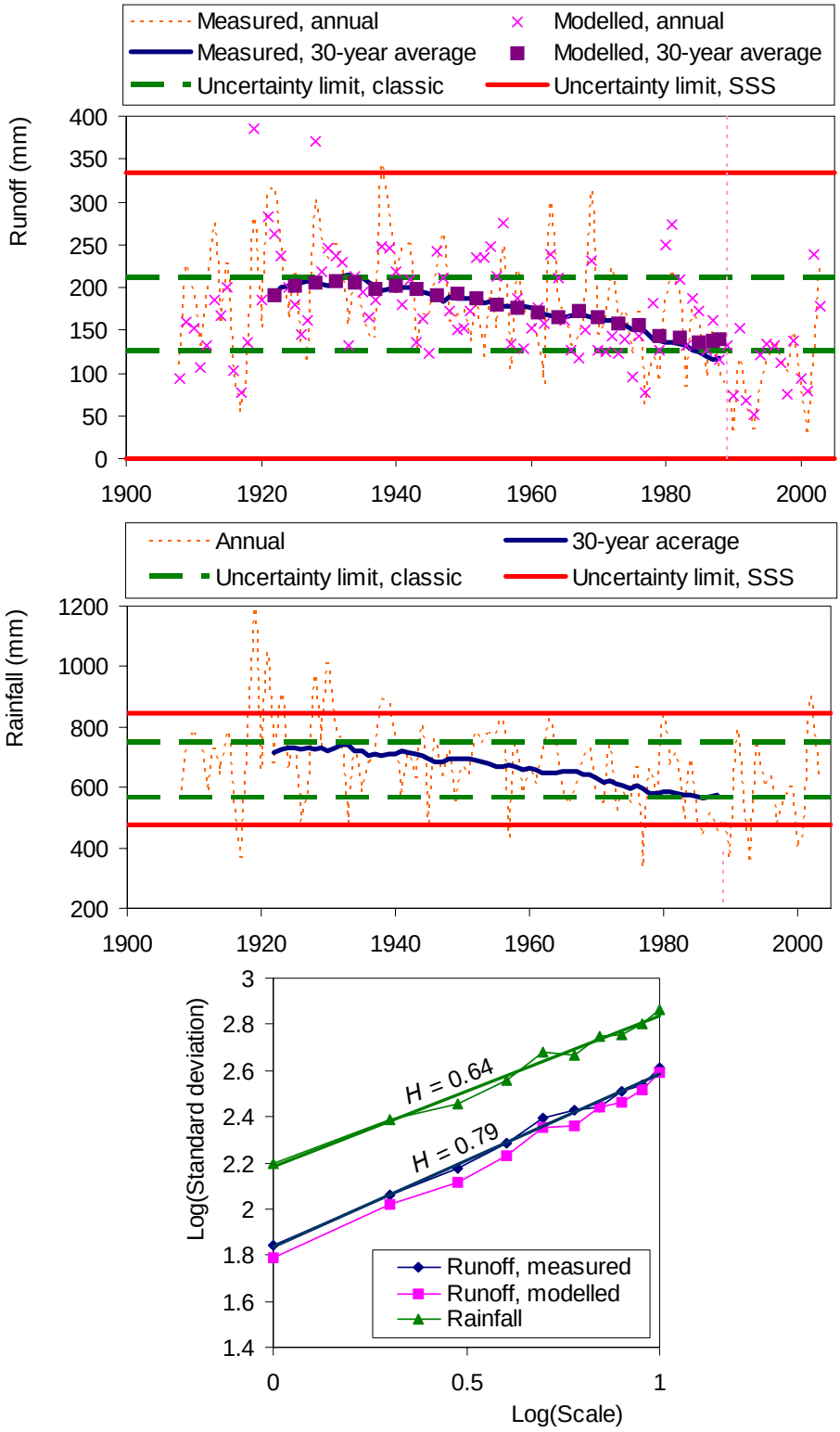

Figure 1 (Up) Plot of the Boeoticos Kephisos river runoff series, both measured and modelled, in annual and 30-year time scales, and of the 95% confidence limits for the 30-year scale, estimated by Monte Carlo simulation. (Middle) Plot of the rainfall series at the same catchment in annual and 30-year time scales, and of the corresponding 95% confidence limits for the 30-year scale. (Down) Aggregated standard deviation plot of the series.

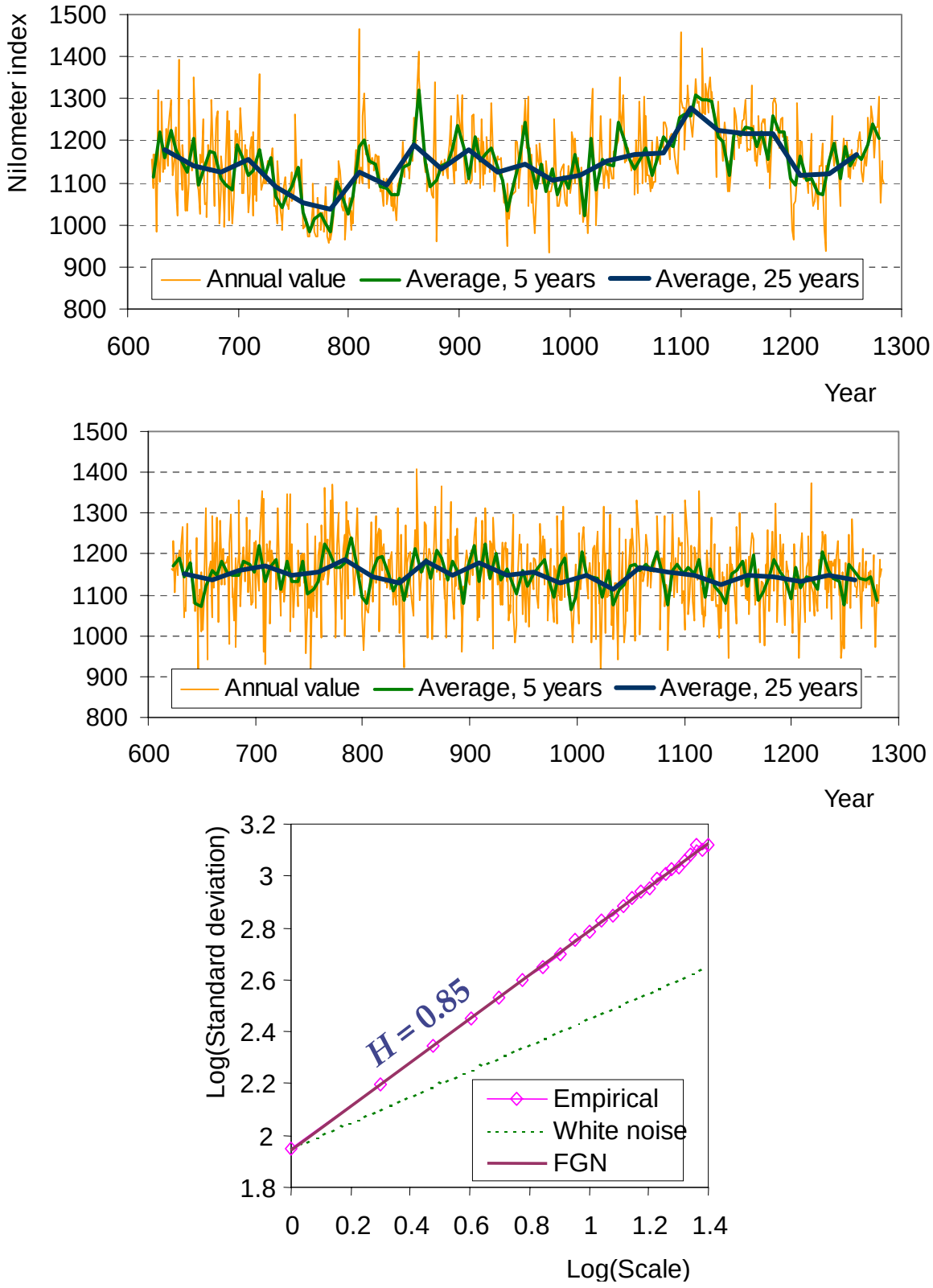

Figure 2 (Up) Plot of the Nilometer series indicating the annual minimum water level of the Nile River for the years 622 to 1284 A.D. (663 years); (middle) a synthetic white noise series, for comparison; (down) aggregated standard deviation plot of the series.

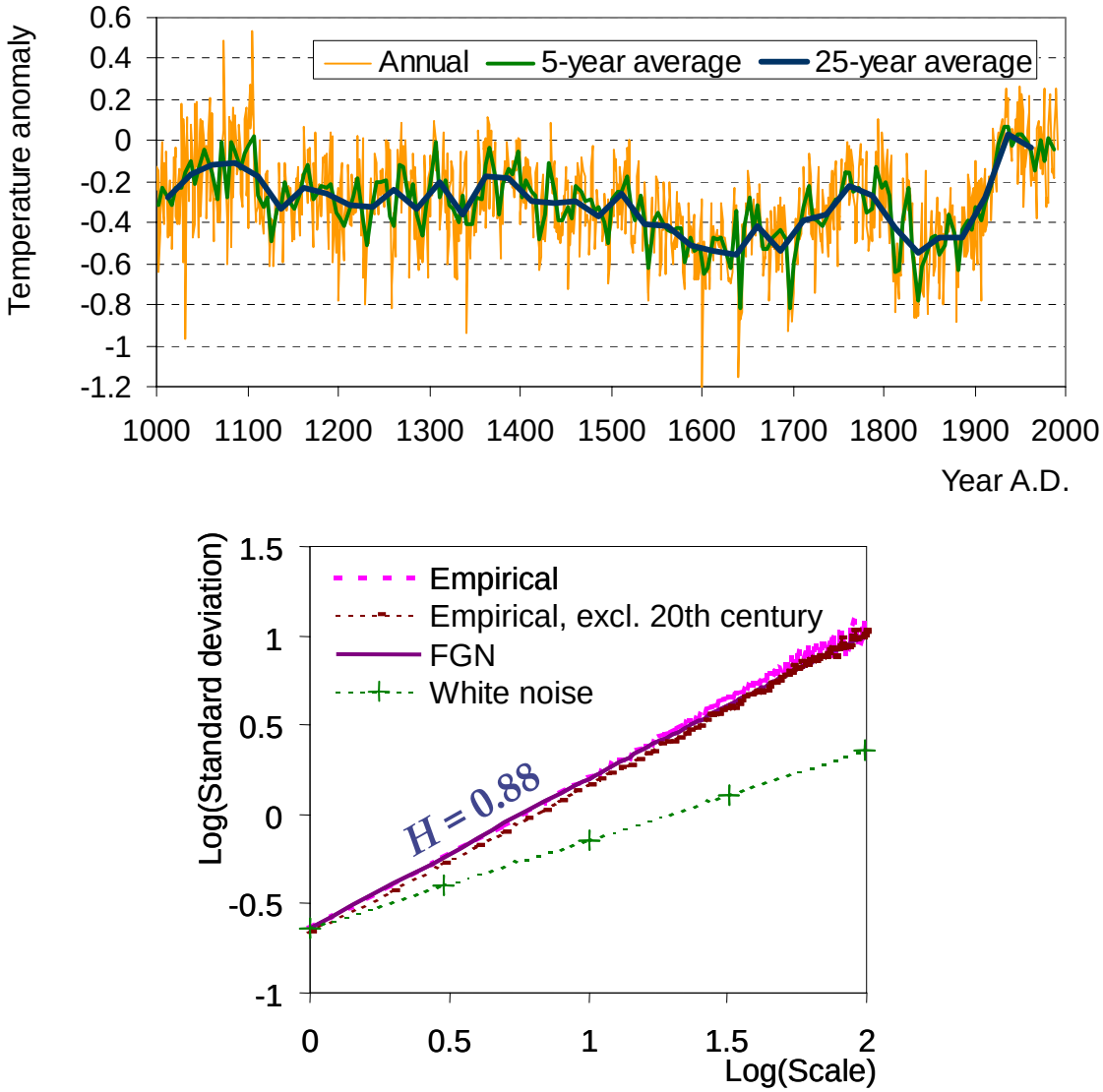

Figure 3 (Up) Plot of the Northern Hemisphere temperature anomalies in °C with reference to 1961–1990 mean (992 years, Jones data set); (down) aggregated standard deviation plot of the series.

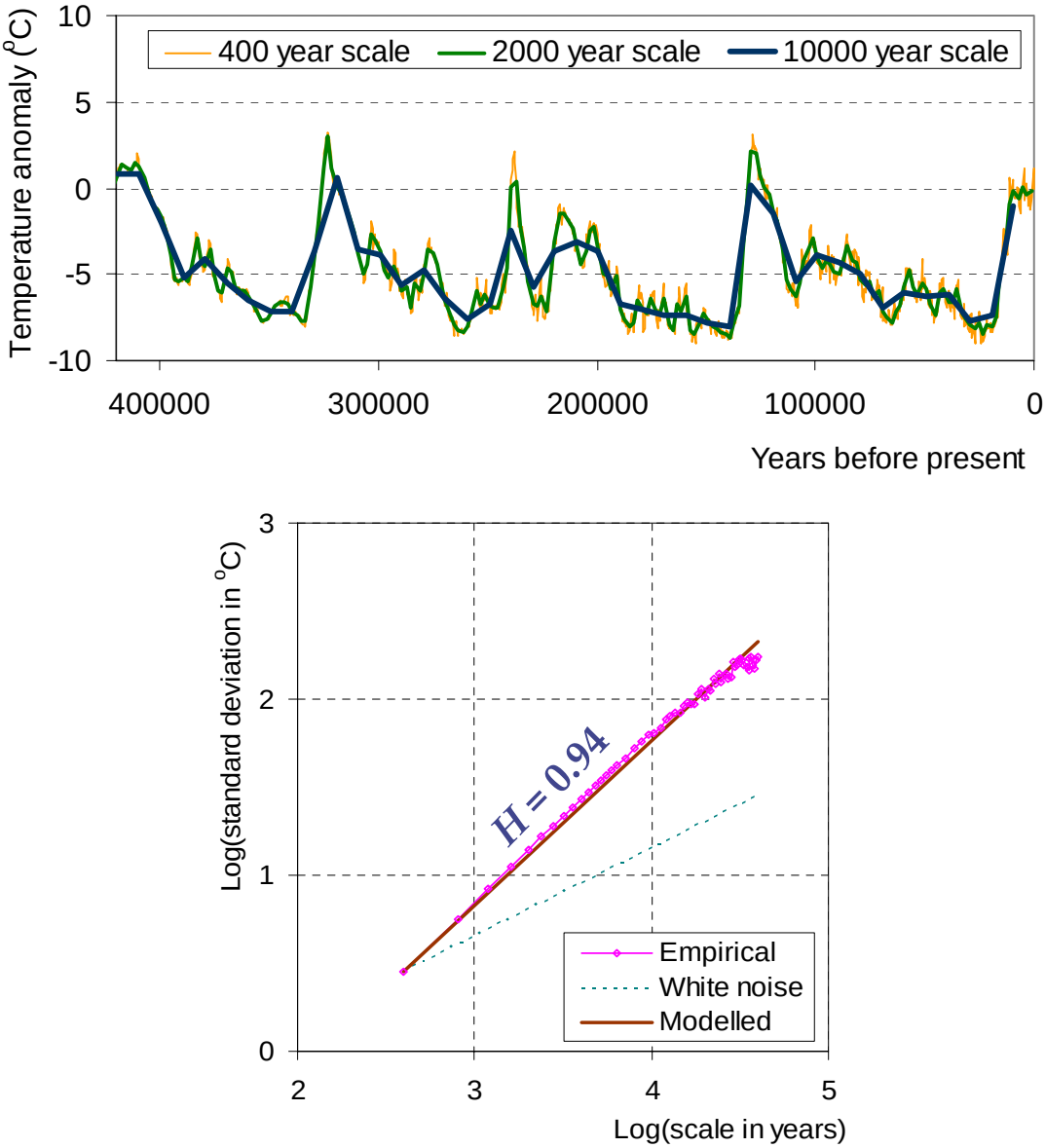

Figure 4 (Up) Plot of the temperature difference, with reference to the mean recent time value, from the Vostok ice core deuterium data set going back to 422 766 years before present; (down) aggregated standard deviation plot of the series.

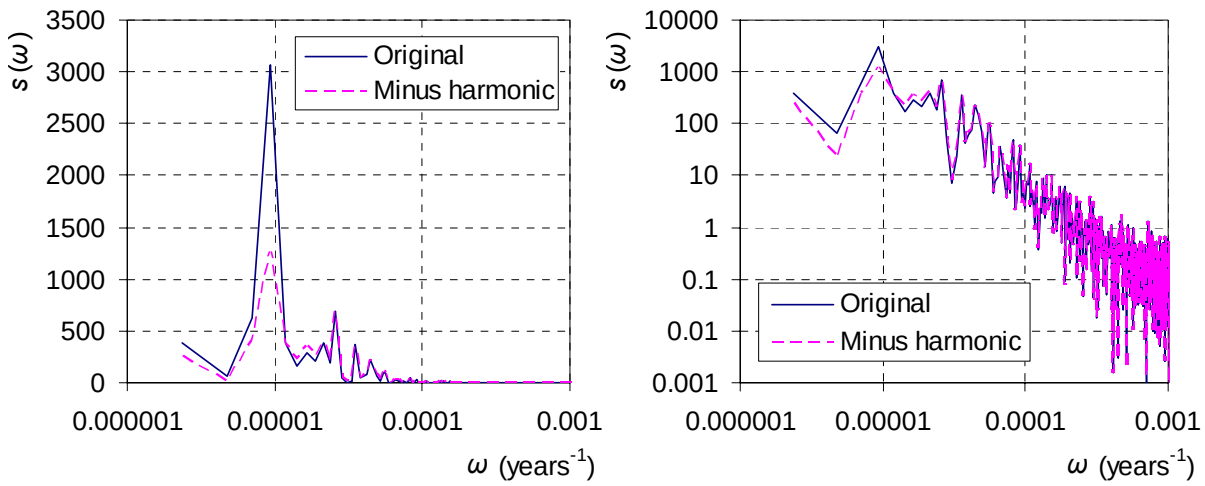

Figure 5 Periodogram of the Vostok temperature time series in Cartesian (left) and logarithmic (right) ordinates.

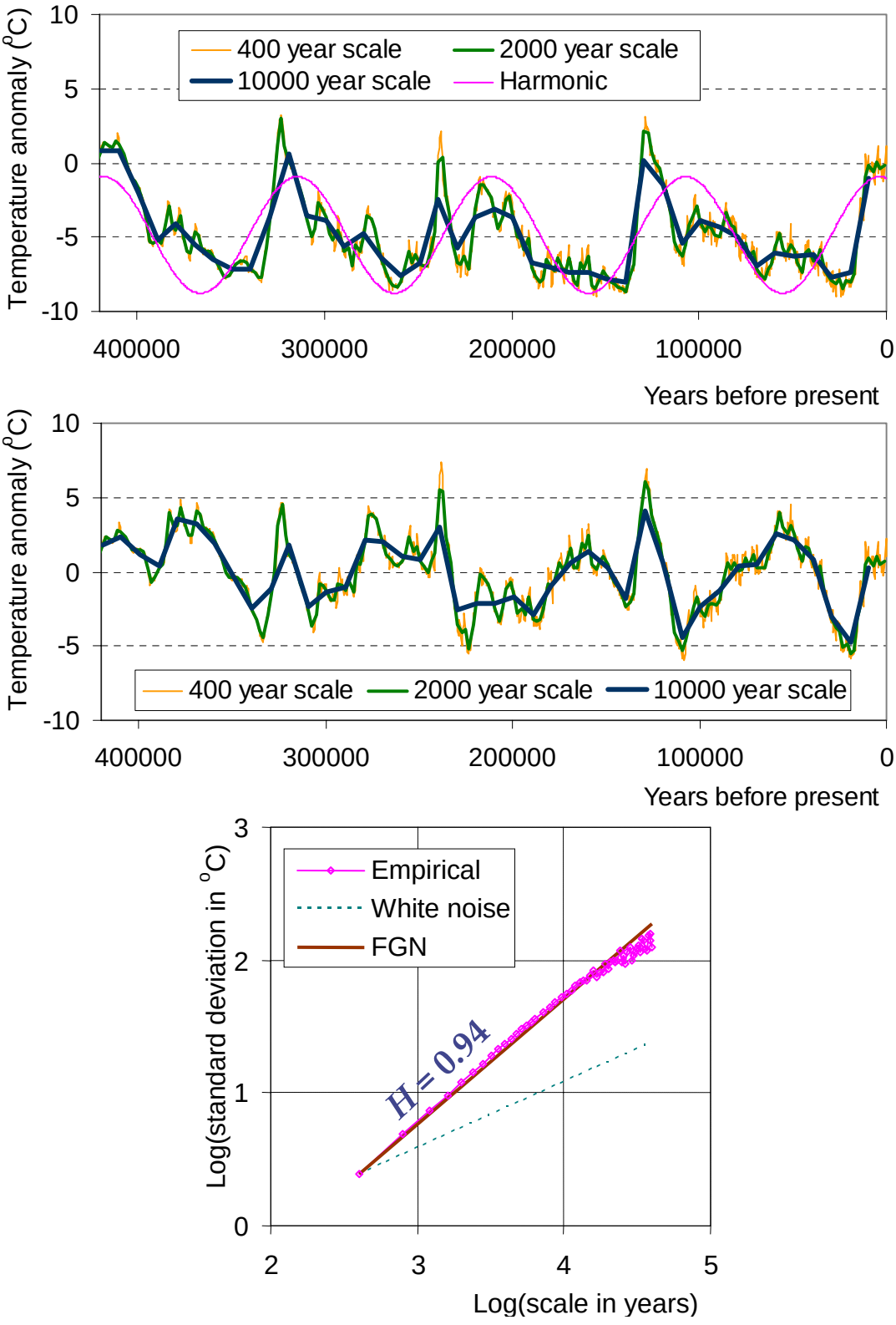

Figure 6 (Up) Fitting of the principal harmonic for the temperature difference of the Vostok data set; (middle) plot of the adapted, by subtraction of the principal harmonic, temperature difference of the Vostok data set; (down) aggregated standard deviation plot of the adapted series.

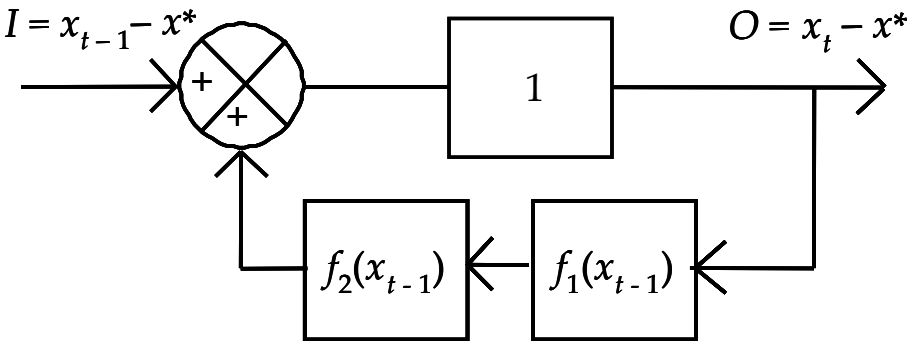

Figure 7 Schematic of a simplified representation of a climatic system with a feedback loop including a positive and a negative reaction.

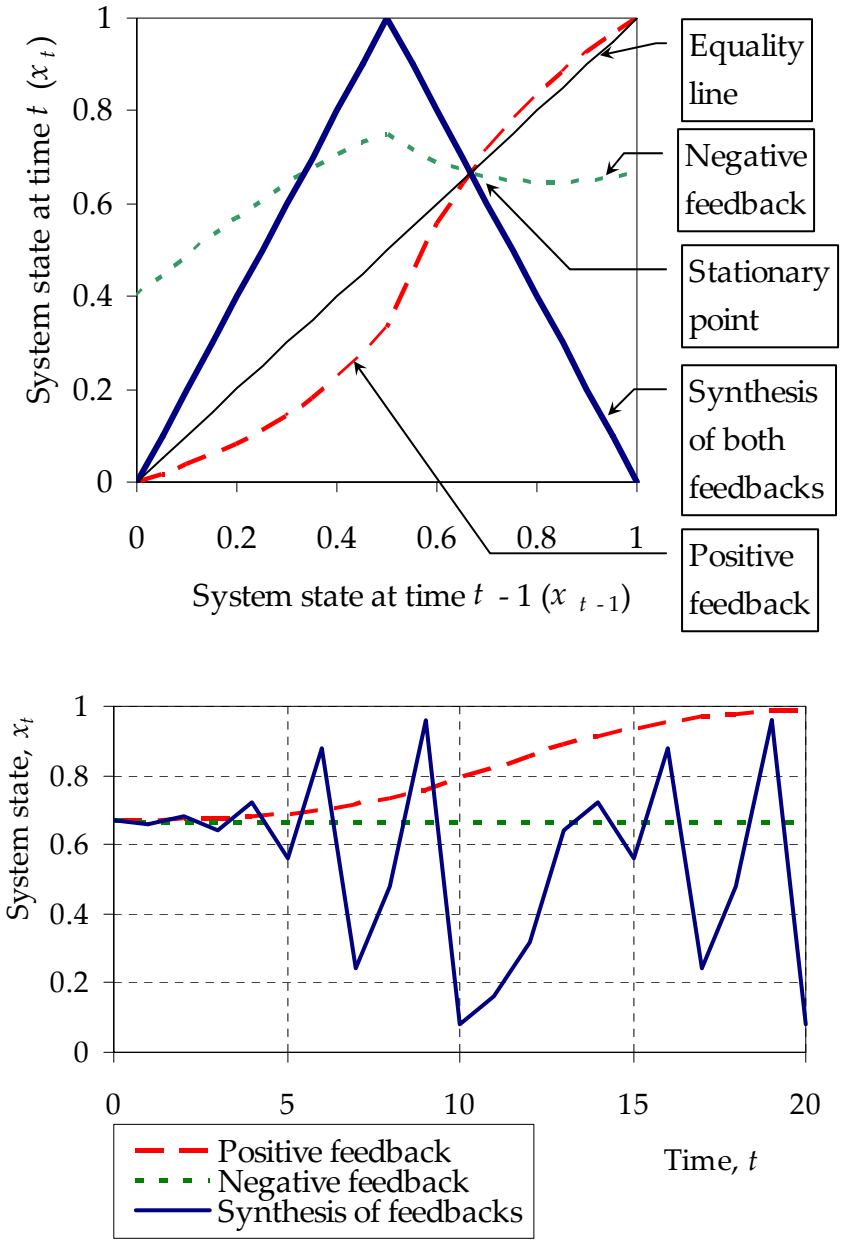

Figure 8 (Up) Schematic of the dynamics of a system subject to a feedback loop with a positive and a negative reaction; (down) evolution of the system under the positive, negative or both reactions, when it starts from very close to its fixed point ($x^* = 2/3$, $x_0 = 0.67$).

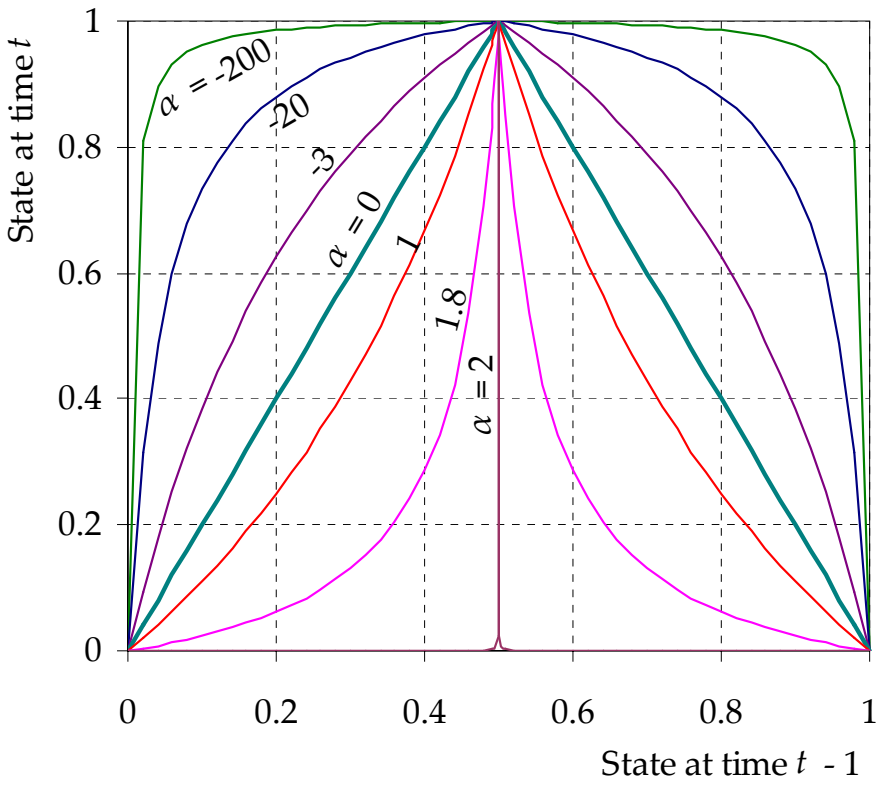

Figure 9 The generalised tent map for different values of its parameter α.

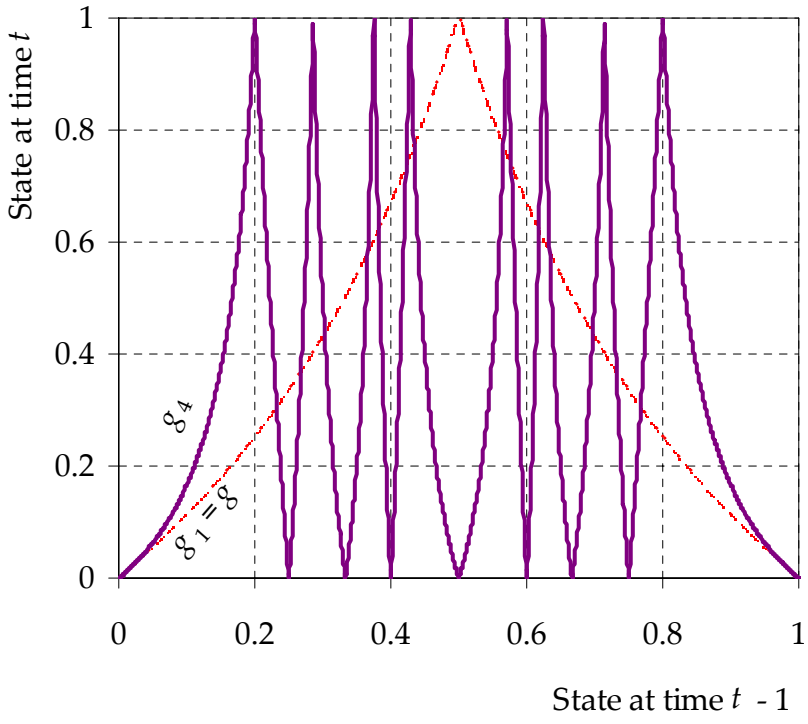

Figure 10 Synthesis of four generalised tent maps for $\alpha = 1$.

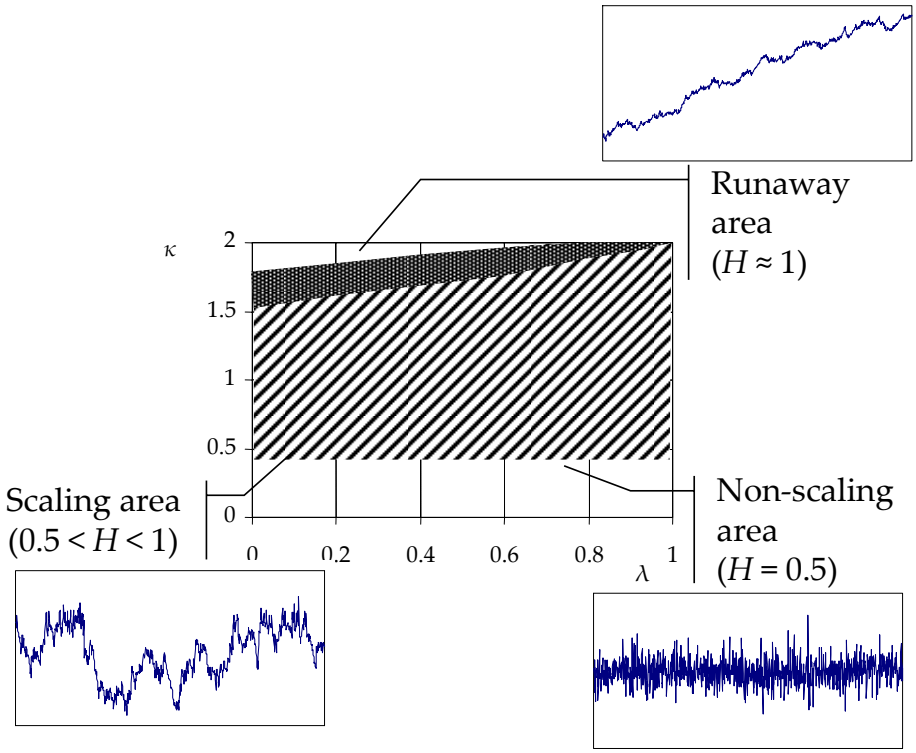

Figure 11 Schematic of the general behaviour of the double tent map in terms of the ranges of its parameters κ and λ. The shaded area corresponds to $n = 1$ and the dark area to $n = 4$.

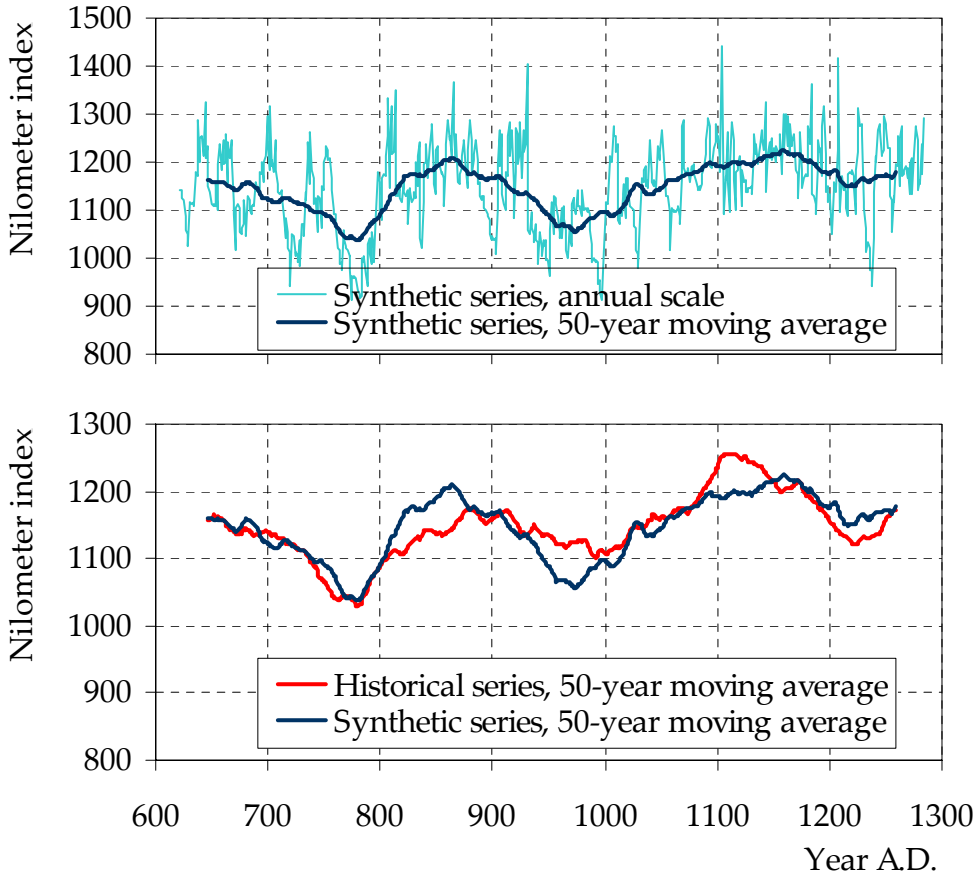

Figure 12 (Up) Plot of the synthetic time series generated by the toy model fitted to the Nilometer data set; (down) comparison of the synthetic and original time series in terms of their 50-year moving averages.

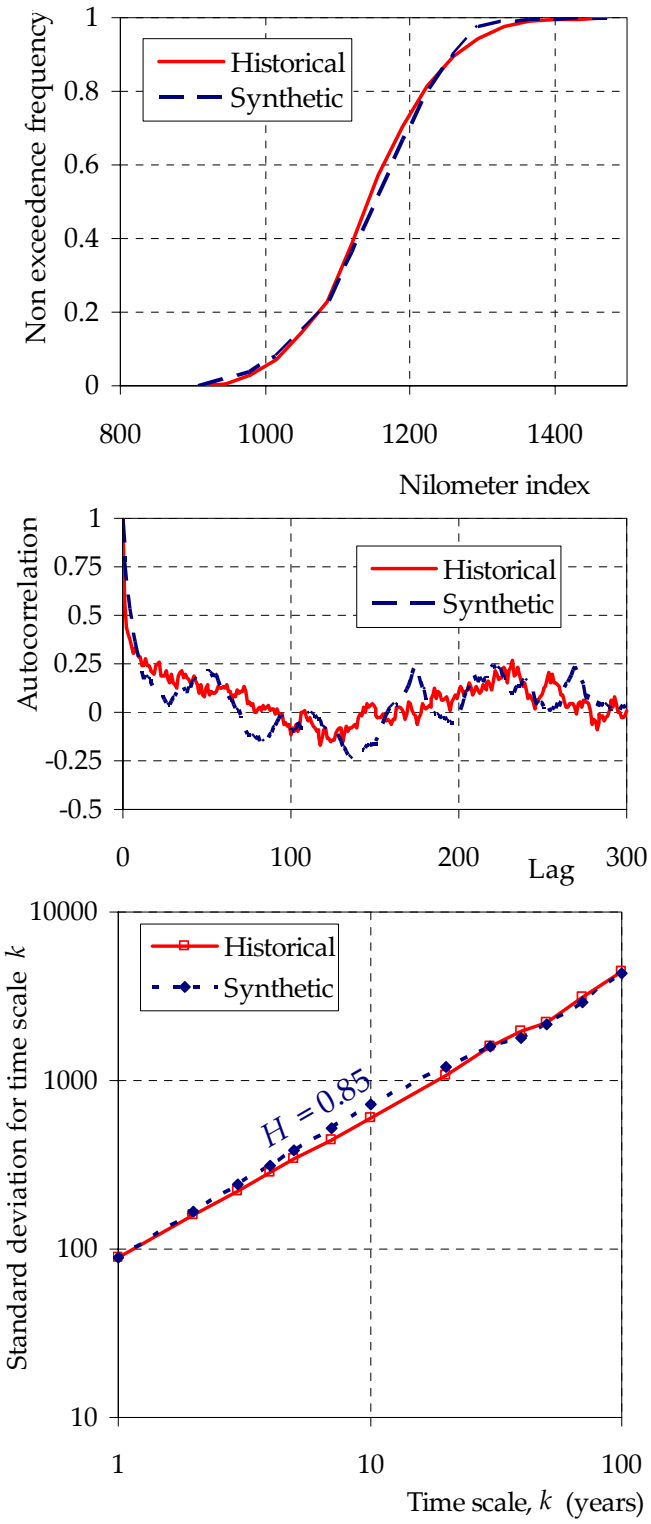

Figure 13 Comparison of statistical properties of the original Nilometer time series and the synthetic one of Figure 12: (up) distribution function; (middle) autocorrelogram; (down) aggregated standard deviation plot.

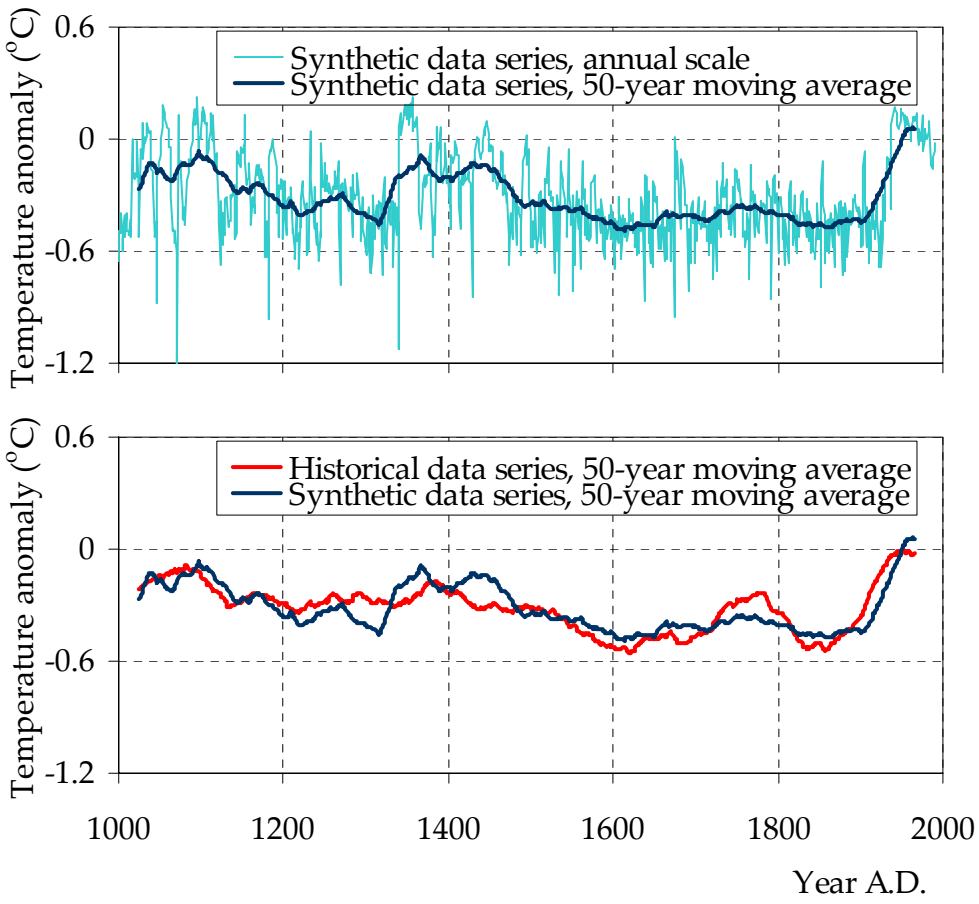

Figure 14 (Up) Plot of the synthetic time series generated by the toy model fitted to the Jones data set; (down) comparison of the synthetic and original time series in terms of their 50-year moving averages.

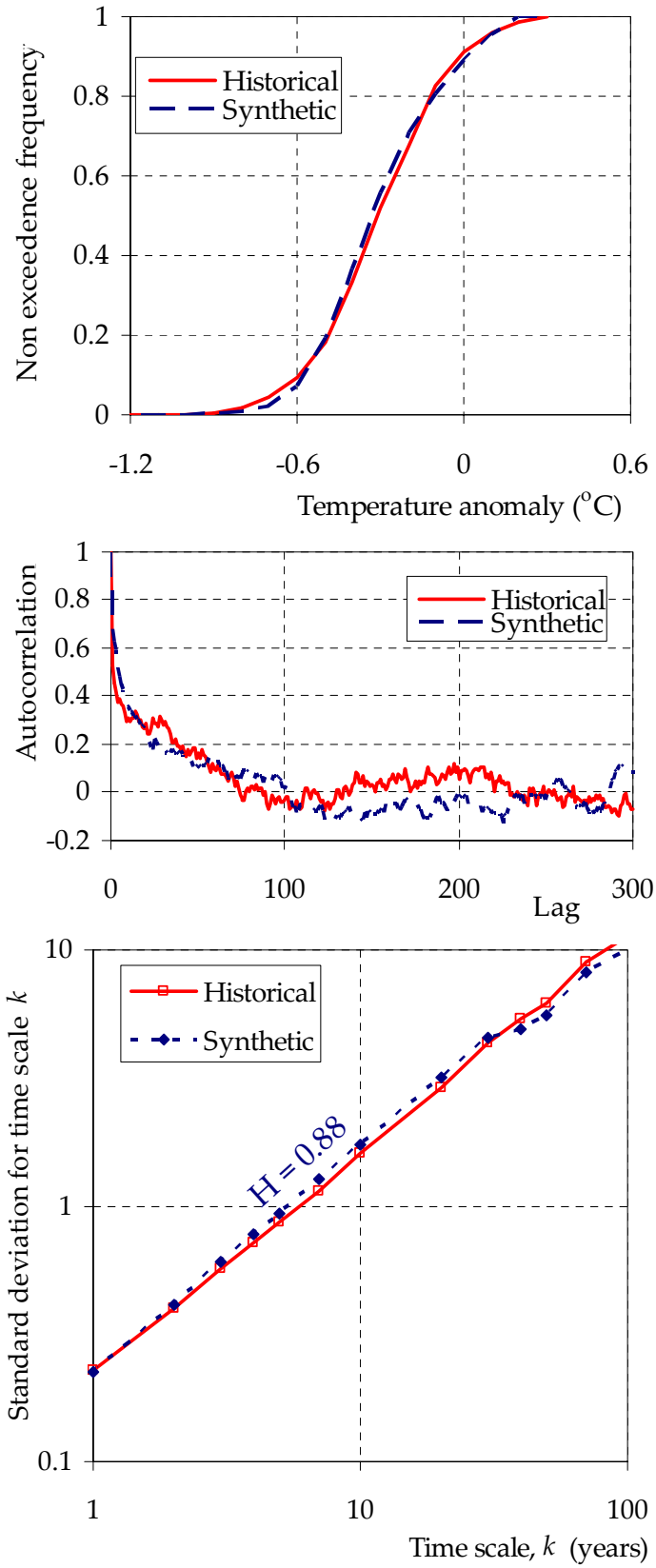

Figure 15 Comparison of statistical properties of the original Jones time series and the synthetic one of Figure 14: (up) distribution function; (middle) autocorrelogram; (down) aggregated standard deviation plot.

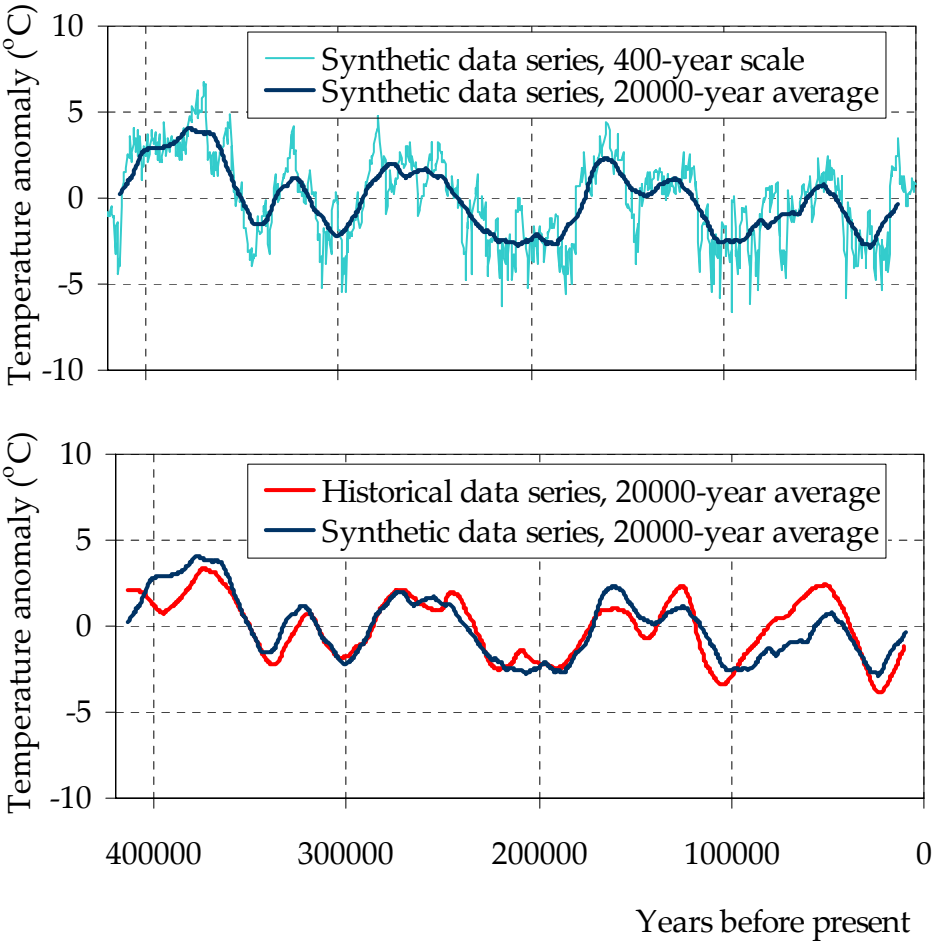

Figure 16 (Up) Plot of the synthetic time series generated by the toy model fitted to the adapted Vostok data set; (down) comparison of the synthetic and original time series in terms of their 20 000-year moving averages.

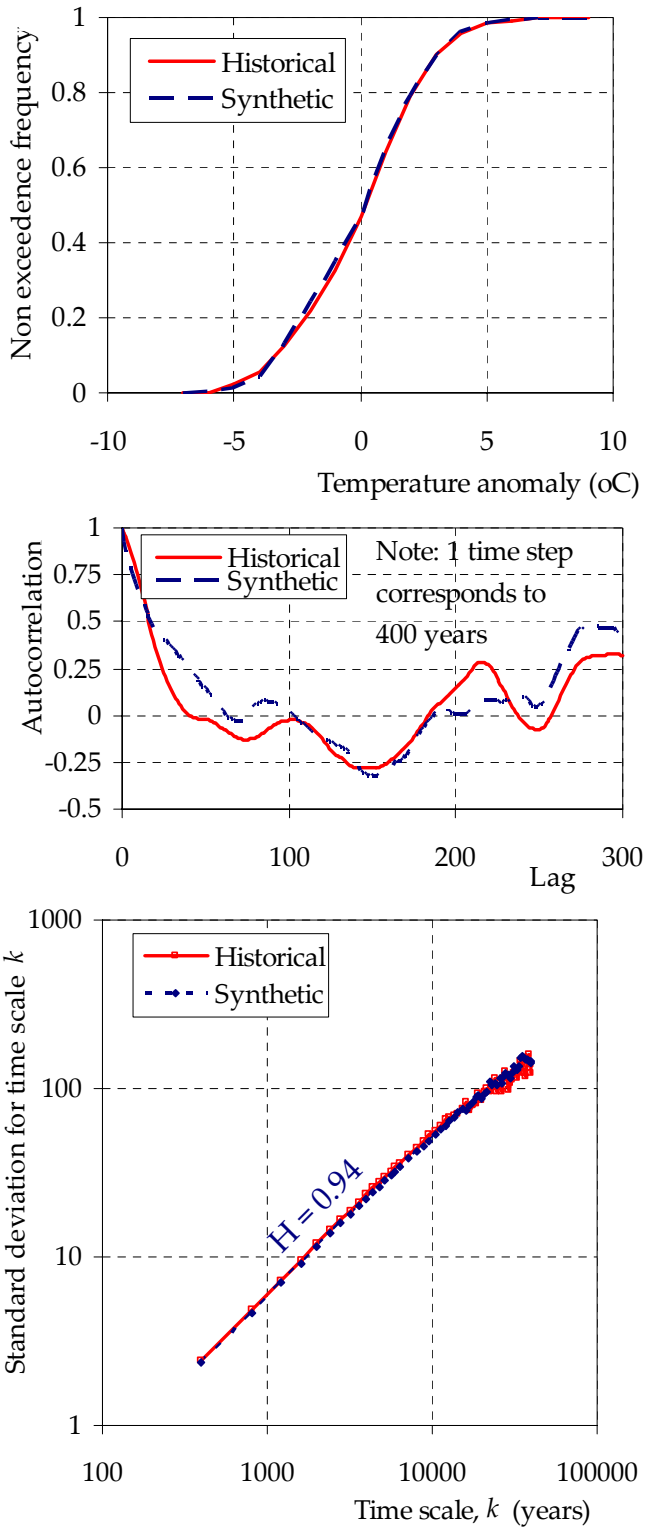

Figure 17 Comparison of statistical properties of the adapted Vostok time series and the synthetic one of Figure 16: (up) distribution function; (middle) autocorrelogram; (down) aggregated standard deviation plot.

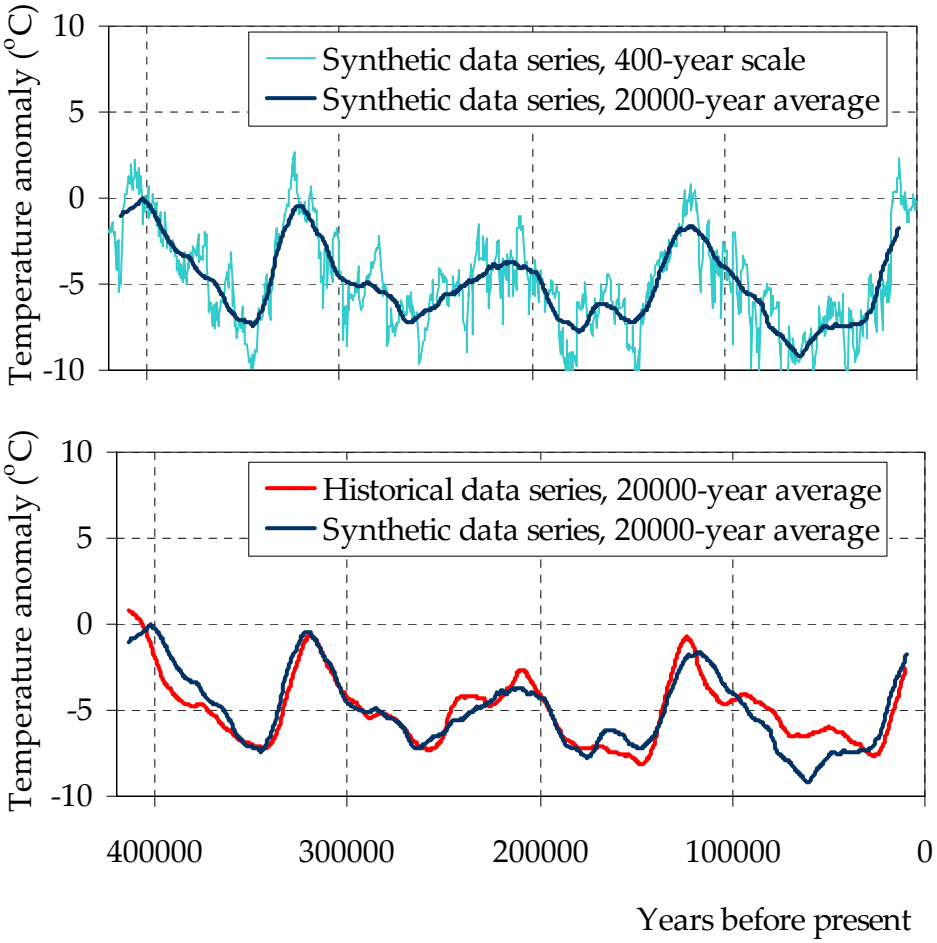

Figure 18 (Up) Plot of the synthetic time series of Figure 16 to which the harmonic with period 103 598 years has been added; (down) comparison of this series with the original Vostok data series in terms of their 20 000-year moving averages.

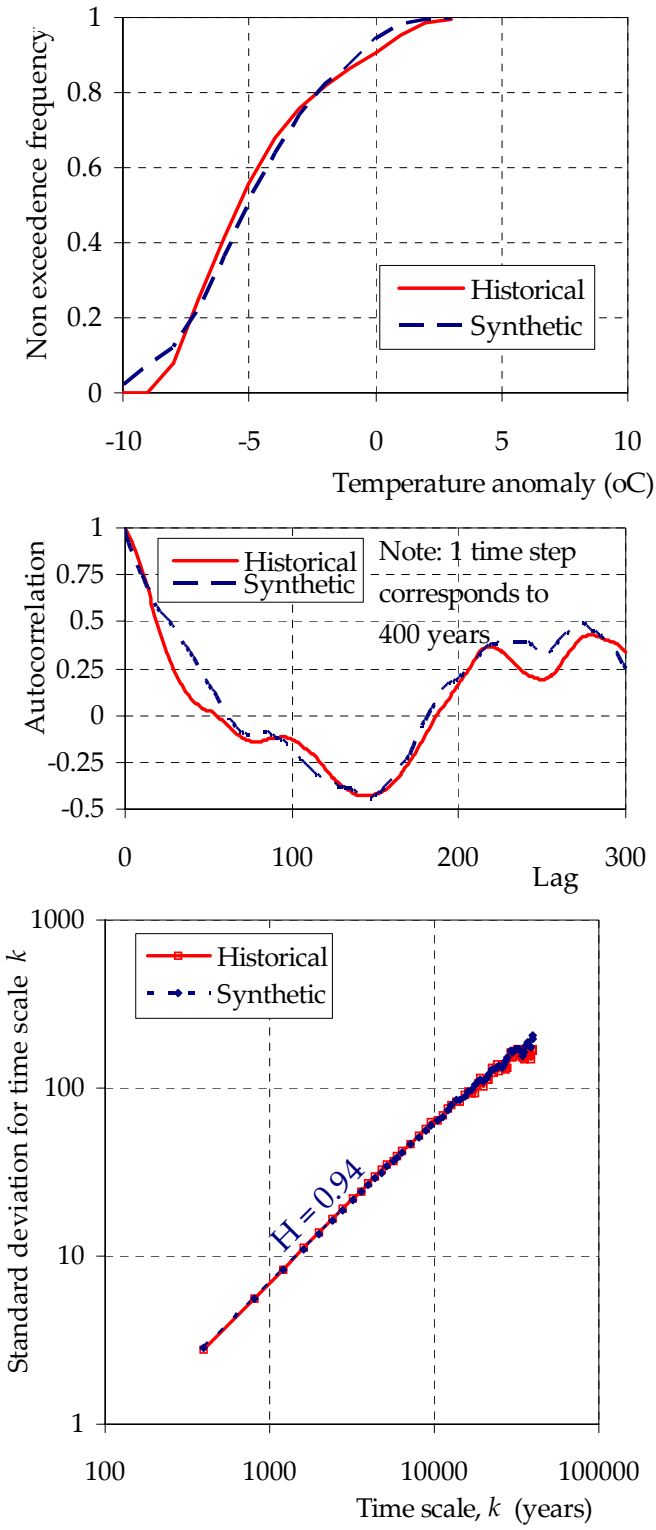

Figure 19 Comparison of statistical properties of the original Vostok time series and the synthetic one of Figure 18: (up) distribution function; (middle) autocorrelogram; (down) aggregated standard deviation plot.

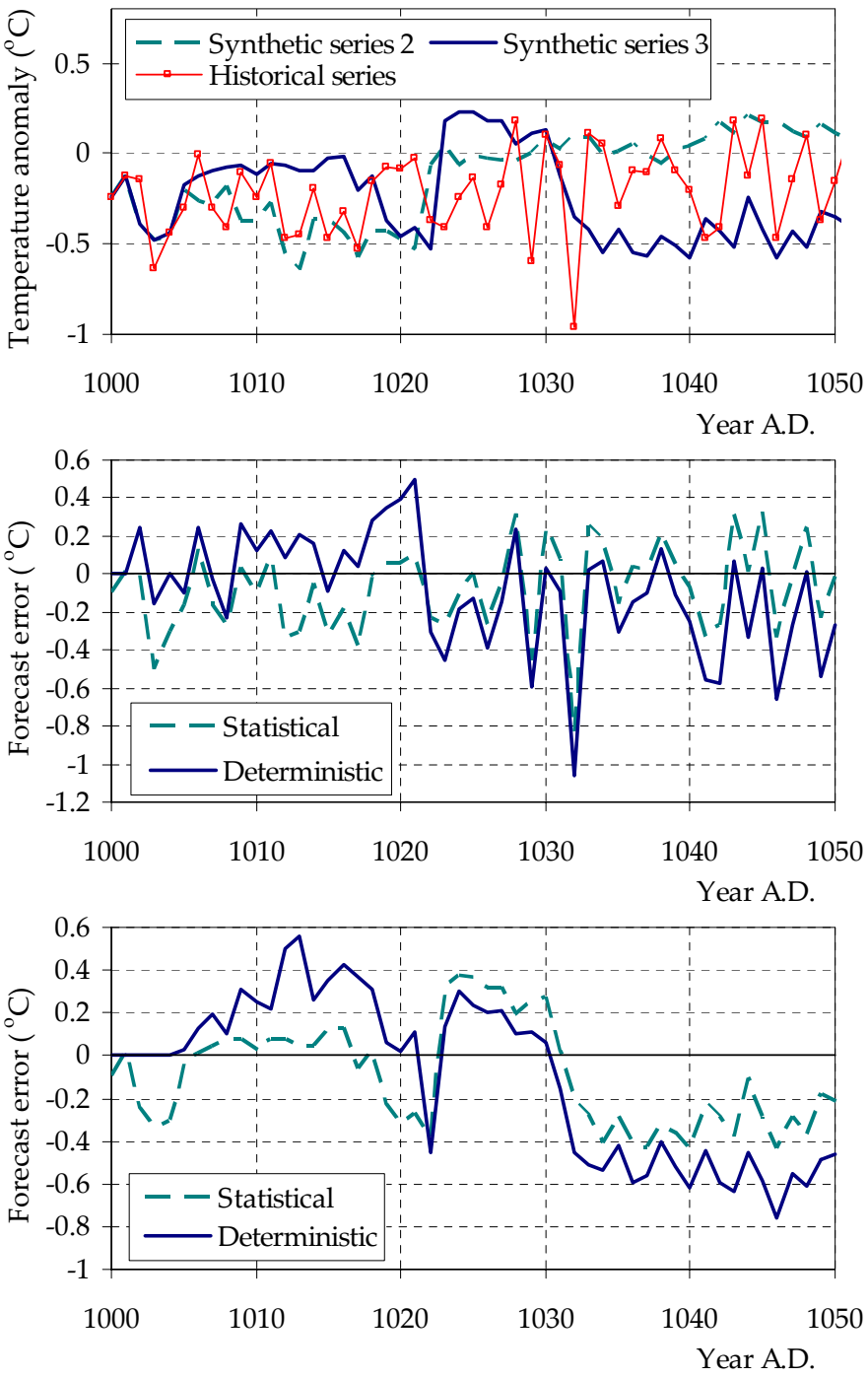

Figure 20 (Up) Plot of the first 50 years of evolution of the historical Jones data series and two synthetic time series (synthetic series 2 and 3), similar to that of Figure 14 (synthetic series 1) but with initial values u_0 and α_0 estimated so that the synthetic series match the historical one at the first two values with the only difference between series 2 and 3 being that the initial value α_0 in the latter is greater by 0.00001% than in the former; (middle) comparison of forecast errors of two forecast methods, (a) statistical, in which the forecast is the average of synthetic series 2 for the 50-year period, and deterministic, in which the forecast is the synthetic series 2; (down) same as in the middle panel but assuming that the actual evolution is that of synthetic series 3.

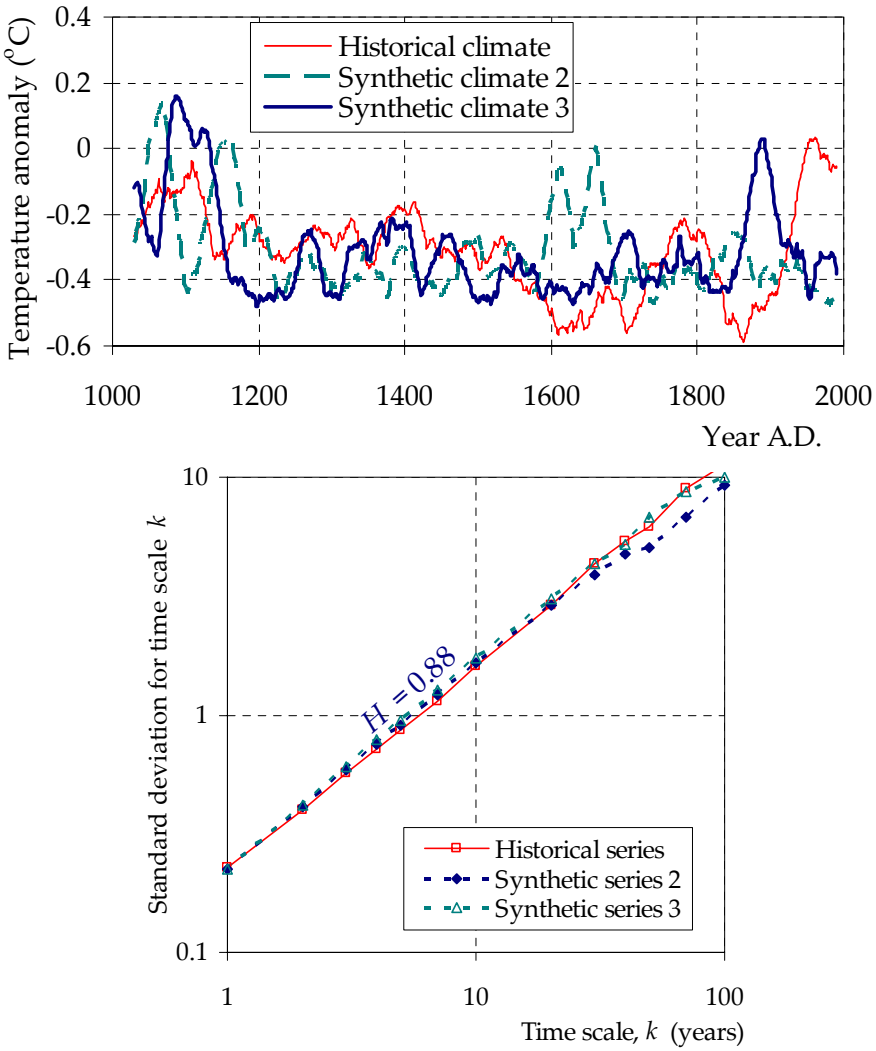

Figure 21 (Up) Comparison of the synthetic series 2 and 3 of Figure 20, and the original Jones series in terms of their moving averages of the past 30 years for all the 1000-year period; (down) comparison of the aggregated standard deviation plots of the three series.

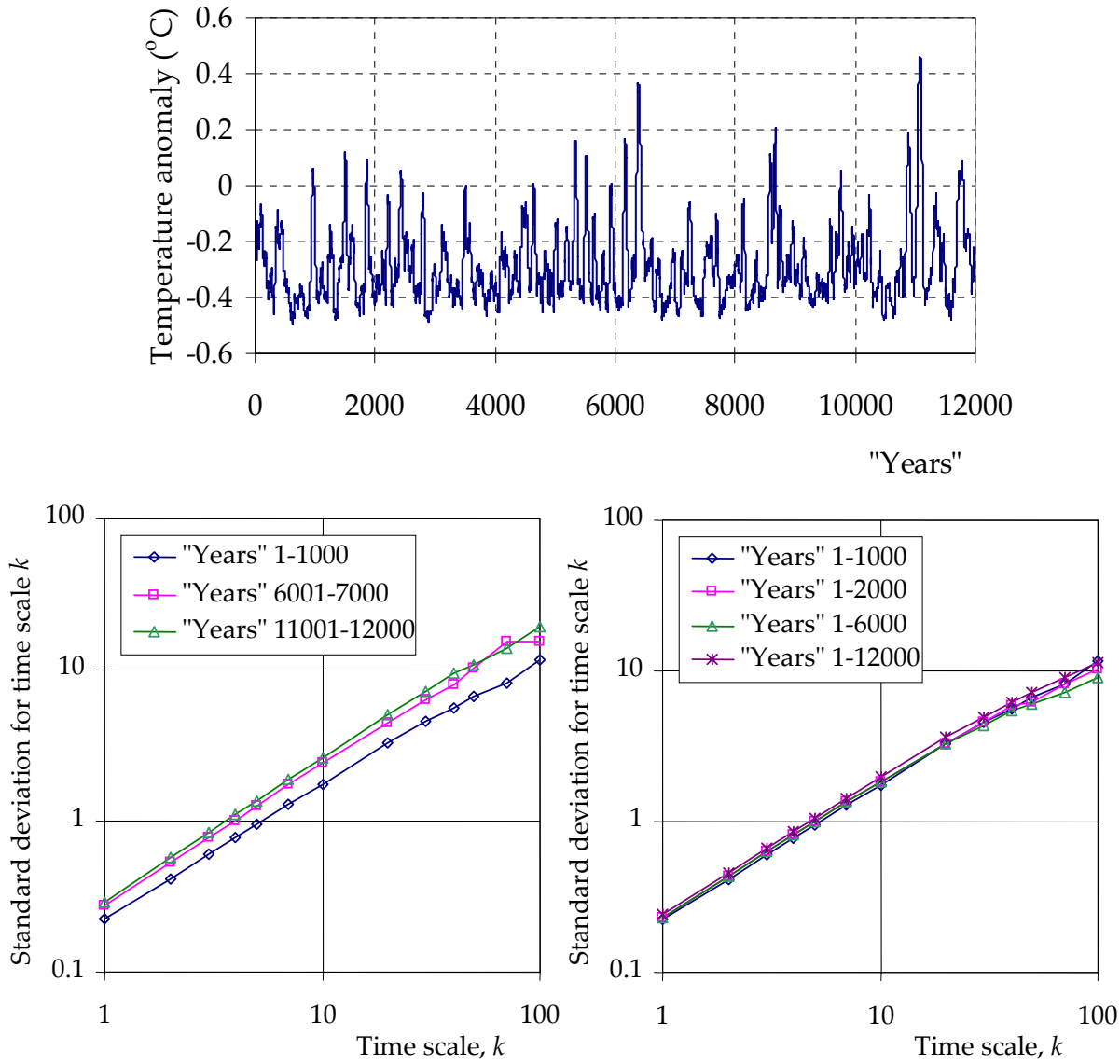

Figure 22 (Up) Plot of the 50-year moving average of the synthetic time series of Figure 14, corresponding to the Jones data set, but extended to the length 12 000 "years"; (down) aggregated standard deviation plots of several parts of the 12 000-year series.

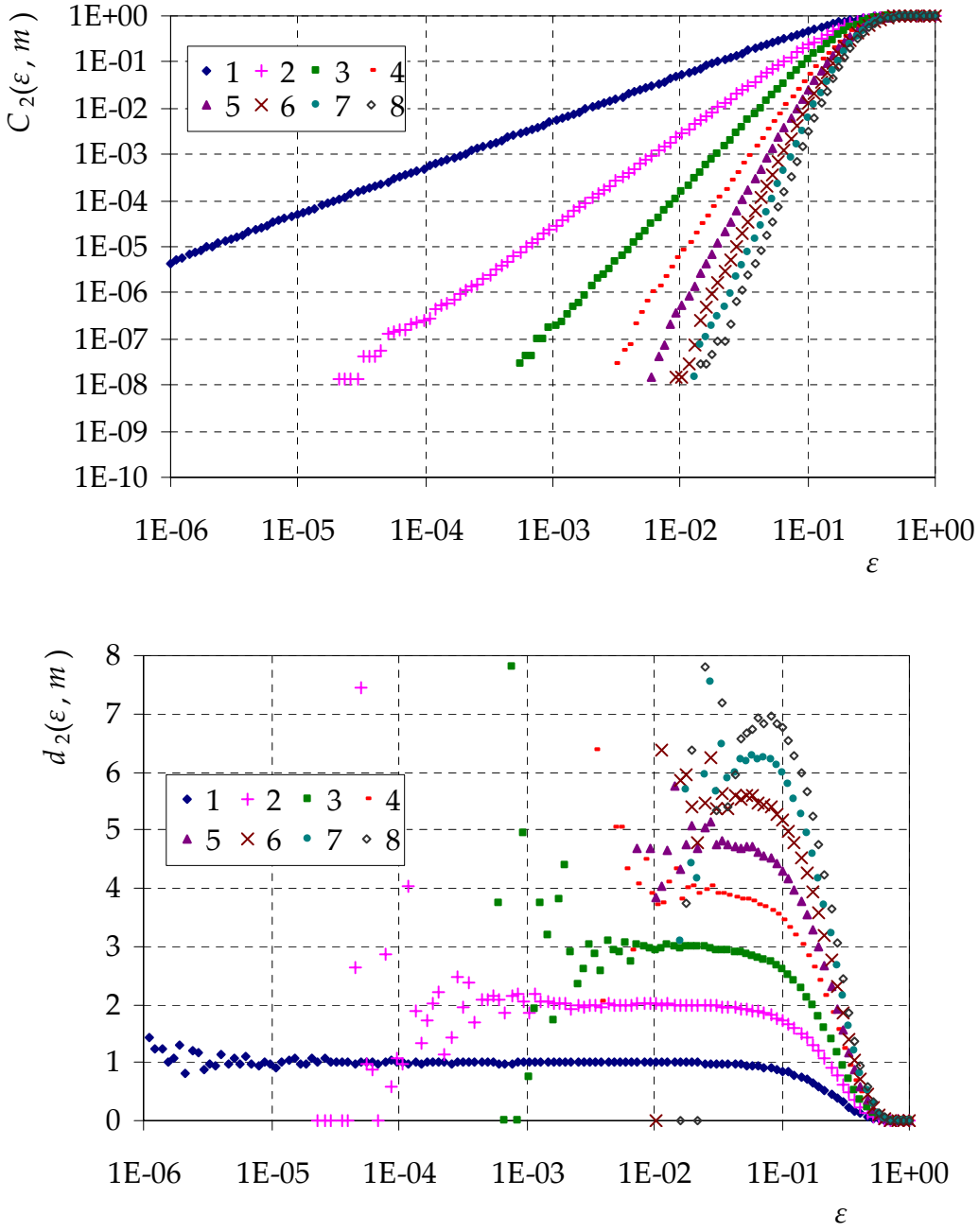

Figure 23 Plots of the correlation sums $C_2(\varepsilon, m)$ (up) and their local slopes $d_2(\varepsilon, m)$ (down) vs. the scale length ε for embedding dimension m = 1 to 8, for the 12 000-year synthetic time series of Figure 22 corresponding to the Jones data set.